Isolated chronic mucocutaneous candidiasis

due to a novel duplication variant of *IL17RC*

Kosuke Noma,[1] Miyuki Tsumura,[1] Tina Nguyen,[2,3] Takaki Asano,[1] Fumiaki Sakura,[1] Moe Tamaura,[1] Yusuke Imanaka,[1] Yoko Mizoguchi,[1] Shuhei Karakawa,[1] Seiichi Hayakawa,[1] Takayo Shoji,[4] Junichi Hosokawa,[5] Kazushi Izawa,[6] Yun Ling,[7] Jean-Laurent Casanova,[8-12] Anne Puel,[8-10] Stuart G Tangye,[2,3] Cindy S Ma,[2,3] Osamu Ohara,[5] Satoshi Okada,[1,*]

1. Department of Pediatrics, Graduate School of Biomedical & Health Sciences, Hiroshima University, Hiroshima, Japan
2. Immunology Program, Garvan Institute of Medical Research, Darlinghurst, NSW, Australia.
3. School of Clinical Medicine, Faculty of Medicine and Health, UNSW Sydney, Kensington, NSW, Australia.
4. Division of Pediatric Infectious Diseases, Shizuoka Children's Hospital, Japan
5. Kazusa DNA Research Institute, Kisarazu, Chiba, Japan
6. Department of Pediatrics, Kyoto University Graduate School of Medicine, Kyoto, Japan
7. Department of Infectious Disease, Shanghai Public Health Clinical Center Shanghai, China
8. Laboratory of Human Genetics of Infectious Diseases, Necker Branch, INSERM U1163, Necker Hospital for Sick Children, Paris, France.
9. University of Paris Cité, Imagine Institute, Paris, France.
10. St. Giles Laboratory of Human Genetics of Infectious Diseases, Rockefeller Branch, The Rockefeller University, New York, NY, USA.
11. Howard Hughes Medical Institute, New York, NY, USA.
12. Department of Pediatrics, Necker Hospital for Sick Children, Paris, France, EU

*Corresponding author:

Satoshi Okada, MD, PhD, Department of Pediatrics, Hiroshima University Graduate School of Biomedical and Health Sciences, 1-2-3 Kasumi, Minami-ku, Hiroshima 734-8551, Japan.

Tel: +81-82-257-5212 Fax: +81-82-257-5214 E-mail: sokada@hiroshima-u.ac.jp

Abstract

Purpose

Inborn errors of the IL-17A/F-responsive pathway lead to chronic mucocutaneous candidiasis (CMC) as a predominant clinical phenotype, without other significant clinical manifestations apart from mucocutaneous staphylococcal diseases. Amongst inborn errors affecting IL-17-dependent immunity, autosomal recessive (AR) IL-17RC deficiency is a rare disease with only three kindreds described to date. The lack of an *in vitro* functional evaluation system of *IL17RC* variants renders its diagnosis difficult. We sought to characterize a seven-year-old Japanese girl with CMC carrying a novel homozygous duplication variant of *IL17RC* and establish a simple *in vitro* system to evaluate the impact of this variant.

Methods

Flow cytometry, qPCR, RNA-sequencing, and immunoblotting were conducted, and an *IL17RC*-knockout cell line was established for functional evaluation.

Results

The patient presented with oral and mucocutaneous candidiasis without staphylococcal diseases since the age of three months. Genetic analysis showed that the novel duplication variant (Chr3: 9,971,476-9,971,606 dup (+131bp)) involving exon 13 of *IL17RC* results in a premature stop codon (p.D457Afs*16 or p.D457Afs*17). Our functional evaluation system revealed this duplication to be loss-of-function and enabled discrimination between loss-of-function and neutral *IL17RC* variants. The lack of response to IL-17A by the patient's SV40-immortalized fibroblasts was restored by introducing WT-*IL17RC*, suggesting that the genotype identified is responsible for her clinical phenotype.

Conclusions

The clinical and cellular phenotype of the current case of AR IL-17RC deficiency supports a previous report on this rare disorder. Our newly established evaluation system will be useful for diagnosis of AR IL-17RC deficiency, providing accurate validation of unknown *IL17RC* variants.

Abbreviations used:

CMC Chronic mucocutaneous candidiasis

AD Autosomal dominant

AR Autosomal recessive

IL Interleukin

Th T helper

Tfh T follicular helper

IEI	Inborn errors of immunity
NGS	Next generation sequencing
WT	Wild-type
SEFIR	Similar expression to fibroblast growth factor genes and IL-17R
pLOF	Predicted to be loss-of-function

Key words: Chronic mucocutaneous candidiasis, isolated CMC, IL-17 immunity, IL-17RC, knockout cell line, inborn error of immunity

Introduction

Chronic mucocutaneous candidiasis (CMC) is a condition characterized by recurrent or persistent superficial infections caused by *Candida spp*., mainly *Candida albicans* (1–4). Studies of patients with CMC have revealed that interleukin (IL)-17 immunity, which involves T helper 17 (Th17) cells and IL-17 signaling, plays a pivotal role in immune defense against mucocutaneous *Candida* infections in humans (3,5). Patients with autosomal dominant (AD) or autosomal recessive (AR) hyper-IgE syndrome due to dominant-negative variants of *STAT3* or *IL6ST* or biallelic variants of *ZNF341* (6–12), AD STAT1 gain-of-function (13–17), AD JNK1 deficiency (18), or AR deficiencies of IL-12p40, IL-12Rβ1, IL-23R (6,19–21), CARD9 (22–24), or RORγT (25) present with CMC as one of the main infectious manifestations, with complications due to susceptibility to other pathogens, autoimmune manifestations, and/or cancers (4,26). Such patients are categorized as having syndromic CMC and commonly show reduced circulating Th17 cell proportions due to impaired differentiation, proliferation, and/or survival (4,5).

Isolated CMC refers to patients with CMC as the predominant clinical phenotype without other significant clinical manifestations (1,4,5,27). However, some patients with isolated CMC may develop mucocutaneous *Staphylococcus aureus* infections (27–29). The discovery of patients with isolated CMC and inborn errors of immunity (IEI) has greatly contributed to our understanding of both the molecular and cellular bases of CMC. Indeed, mono- or biallelic deleterious variants of *IL17F*, *IL17RA*, *IL17RC*, and *TRAF3IP2* (encoding ACT1) have been detected in patients with isolated CMC, and *MAPK8* has been identified in patients with both CMC and a connective tissue disorder (27–34). These five genes are all directly involved in the IL-17A/IL-17F-dependent IL-17RA/IL-17RC-mediated signaling pathway. Clinical and molecular investigations of these patients suggest that host mucocutaneous immunity against *Candida* critically depends on IL-17 immunity. IL-17RA is ubiquitously expressed, whereas IL-17RC is predominantly expressed on epithelial and mesenchymal cells (35–37). The two chains form a dimeric receptor for IL-17A and IL-17F homo- or heterodimers, which are mainly produced by Th17 cells (38). IL-17A and IL-17F (IL-17A/F) binding to their receptors results in recruitment of ACT1, an adapter molecule activating several downstream signaling pathways (35,38), to the cytoplasmic domains of the receptors, leading to release of antimicrobial peptides and cytokines/chemokines such as IL-6, G-CSF, CXCL1 and CXCL8 to control *Candida* infection.

AR IL-17RC deficiency was reported in 2015 in three unrelated patients from three families originating from Argentina and Turkey with isolated CMC and no staphylococcal mucocutaneous manifestations (30). However, additional patients have not yet been reported. Those three patients carried different homozygous nonsense variants, i.e., p.Q138*, p.R376*, and p.Q378*, inherited from heterozygous asymptomatic parents. Fibroblasts from the patients did not exhibit responses to IL-17A/F homo- and heterodimers. We herein report a patient with isolated CMC and a homozygous novel duplication variant of *IL17RC*. In addition, we successfully established a simple *in vitro* system that can accurately assess the functional impact of *IL17RC* variants.

Methods and Materials

Molecular Genetics

Genetic testing was performed after obtaining written informed consent from the participants or their guardians. Genomic DNA was extracted from peripheral blood leukocytes and subjected to NGS based gene panel testing for IEI and Sanger sequencing. The detailed method of gene panel testing was described previously (39). Briefly, paired-end sequence libraries were constructed using the TruSeq DNA PCR Free Library Kit (Illumina). The libraries were subjected to 150-bp paired-end sequencing on the HiSeq X Ten system (Illumina). Reads from the fastq files were aligned to the human reference genome GRCh37/hg19 using Burrows-Wheeler Aligner Software. Duplicate reads were removed using Picard Mark Duplicates. The mapped reads around insertions/deletions (Indels) were realigned by the Genome Analysis Toolkit (GATK) Version 4.0. Variant calling was performed using GATK HaplotypeCaller. The called single-nucleotide variants (SNVs) and Indels were annotated using the SnpEff software 4.3.

Quantitative PCR

Total RNA was extracted from the cell lines with Qiagen RNeasy Mini kit (Qiagen, Hilden, Germany) or SingleShot Cell Lysis Kit (Bio-Rad, Hercules, CA) and reverse transcribed by Superscript III Reverse Transcriptase (Invitrogen, Carlsbad, CA, USA) or iScript Adv cDNA synthesis kit (Bio-Rad, Hercules, CA). All procedures were performed according to the manufacturer's instructions. Quantitative real-time PCR was performed with Taqman Gene Expression Master Mix (Applied Biosystems) and probes (**Table. S1**) on StepOnePlus Real-Time PCR system (Applied Biosystems). The expression levels of each transcript were determined in triplicate and normalized to the level of *GAPDH*. Data analysis was performed with the comparative threshold cycle method (also known as the $2^{-\Delta\Delta Ct}$ method).

Immunoblot analysis

V5-taggerd WT and/or *IL17RC* mutant containing plasmids were introduced into SV40-fibroblasts with lipofection, and were collected 24 hours after transfection. For whole-cell extracts, the cells solubilized with sodium dodecyl sulfate (SDS) buffer (100 mM Tris/HCl, pH 6.8, 4 % SDS, 20% glycerol and 1.2 % 2-mercaptoethanol) and then sonicated. The cell lysates were separated by 10% SDS-PAGE, and proteins were transferred to polyvinylidene fluoride membranes (Merck KGaA, Darmstadt, Germany). After blocking with skimmed milk, the membranes were incubated with primary antibodies against IL-17RC (1:1000, Sigma-Aldrich, HPA019885), V5 (1:1000, Sigma-Aldrich) or β-actin (1:2000, Sigma-Aldrich) at 4°C overnight. Horseradish peroxidase–conjugated goat anti-mouse and anti-rabbit antibodies (GE Healthcare, Buckinghamshire, England) were used as secondary antibodies. Antibody binding was detected with enhanced chemiluminescence reagent (ImmunoStar Zeta reagent, FUJIFILM).

IL17RC knockout HeLa cell preparation

The CRISPR/Cas9 system was used to generate *IL17RC* knockout HeLa cells. Two sgRNA sequences (GGTGCGTAGGCGCCAGCACG and CTGTGACCTCTGTCTGCGTG) targeting the *IL17RC* gene were designed in exon 3 using CRISPRdirect (40). Cloning of the respective sgRNA tandem constructs into pSpCas9(BB)-2A-GFP (PX458) (Addgene plasmid #48138) was performed according to previous reports and confirmed by sequencing (41). Transfection of sgRNA-Cas9 Plasmid into WT HeLa cells was performed using the Neon™ transfection system (Invitrogen/Thermo Fisher Scientific Inc.) according to the manufacturer's instructions. After 48 hours of incubation from transfection, GFP expressing cells were sorted with FACSAria™ III (Becton Dickinson, Franklin Lakes, USA) into single, and expanded under conditions at 37 °C, 5 % CO2. Successful knockout of *IL17RC* was confirmed by direct sequencing of the genomic DNA and quantitative PCR for *IL17RC* of the candidate clones (**Fig.S1A, S1B**).

CXCL1 quantitative PCR using the *IL17RC*-targeted HeLa cell line

The *IL17RC*-deficient HeLa cells were plated in 96-well plates at a density of 1.6 x 10^4 cells/well and incubated for 24 hours and then transfected with mock, pUNO1 vector, WT or *IL17RC* mutant plasmid (20 ng). After 24 hours, the transfected cells were left unstimulated or stimulated with 100 ng/mL recombinant human IL-17A for 4 hours. cDNA was synthesized using total RNA extracted from the cells, and quantitative PCR was performed for *CXCL1*. Expression level of each transcript was determined in triplicate and normalized to the level of *GAPDH*. Data analysis was performed with the comparative threshold cycle method (also known as the $2^{-\Delta\Delta Ct}$ method).

Isolation and functional characterization of human T cells

Naïve and memory $CD4^+$ T cells were isolated by excluding Tregs ($CD4^+CD25^{hi}CD127^{lo}$) then sorting $CD45RA^+CCR7^+$ cells and $CD45RA^-CCR7^{+/-}$ cells, respectively. Purity of the recovered populations was >98%. Sorted naïve and memory $CD4^+$ T cells were cultured at a density of 150-200×10^3 cells/ml in 96-well round-bottom plates with T cell activation and expansion (TAE) beads (anti-CD2/CD3/CD28; Miltenyi Biotech) alone (Th0) or under Th1 (50 ng/ml IL-12; R&D systems), Th2 (1 U/ml IL-4; DNAX), or Th17 (10 ng/ml TGF-β1; PeproTech, 200 ng/ml IL-1β; PeproTech, 200 ng/ml IL-6; PeproTech, 200 ng/ml IL-21; PeproTech, and 200 ng/ml IL-23; PeproTech) polarizing conditions. After 5 days, supernatants were harvested to measure secretion of IL-2, IL-4, IL-5, IL-13, IL-17A, IL-17F, IFN-γ and TNF-α using cytometric bead arrays (Becton Dickinson). IL-22 secretion was measured by ELISA (PeproTech). Intracellular cytokine expression was determined following re-stimulation of cells with phorbol 12-myristate 13-acetate (Sigma-Aldrich) and ionomycin (Sigma-Aldrich) with addition of Brefeldin A (10μg/ml) after 2 hours.

Other materials and methods are described in the "Supplementary Materials".

Results

A sporadic case of CMC

We examined a seven-year-old girl born to Japanese parents from the same city but without any known consanguinity (**Fig. 1A**). The prenatal history was normal, and there was no family history of IEI. From the age of three months onward, the patient developed oral and cutaneous candidiasis, especially at the external eye angle. (**Fig. 1B**). Mucositis of the nasal cavity and vulva was also observed. These symptoms of oral and cutaneous candidiasis responded well to fluconazole treatment, and flare occurred with discontinuation of treatment. Endoscopy examination at the age of seven years revealed that she had esophageal candidiasis (**Fig. 1B**). Antifungal drugs had never been used continuously due to the concern of emerging resistant strains. Her oral and cutaneous candidiasis therefore persisted, though she never developed invasive candidiasis. She had sensitive skin and recurrent sweating rashes, which especially grew worse in summer. Mosquito bites were abnormally swollen, sometimes resembling impetigo. Her growth and development were normal, including hair, nails, teeth, and sweating. She also developed herpes zoster of the left shoulder and right side of the head at the age of six years. Otherwise, she had no episodes indicating susceptibility to severe bacterial or viral diseases. Immunological investigations were unremarkable (**Table. S2**). She was thus given a diagnosis of isolated CMC based on the absence of any phenotypes other than CMC.

Identification of a homozygous novel duplication variant of *IL17RC*

We performed next-generation sequencing (NGS) gene panel testing for IEI using genomic DNA from the patient's leukocytes, revealing an increased number of reads in a region including the entire exon 13 of *IL17RC* (**Fig. 1C**). This finding was not detected by the variant calling system but was identified manually when we directly analyzed the data aligned to the reference genome. Subsequent Sanger sequencing of the patient's DNA identified a homozygous novel duplication variant (Chr3: 9,971,476-9,971,606 dup(+131bp), c.1324_1372dup) of *IL17RC* (**Fig. 1D**). A genetic test of the patient's healthy mother and siblings revealed them to be heterozygous for the variant or wildtype (**Fig. 1D**). A genetic test was not available for the father. This duplication variant was not found in various public databases, such as gnomAD (https://gnomad.broadinstitute.org, v2.1.1) or TOPMED/BRAVO (https://bravo.sph.umich.edu), suggesting that it is a novel and private variant. Analysis of mRNA extracted from the patient's fibroblasts revealed that this variant results in a duplication of 46 (exon13dup_1) or 49 (exon13dup_2) bases *IL17RC* of exon 13 (**Fig. 1E, S1C)**. Both the 46- and 49-base duplications in exon 13 cause a frameshift resulting in a premature stop codon (p.D457Afs*16 or p.D457Afs*17) (**Fig. 1E**). This variant affects a conserved SEFIR (similar expression to fibroblast growth factor genes and IL-17R) domain of IL-17RC, which is essential for signaling to ACT1 (42) (**Fig. 1F**). Additionally, the variant has a high CADD (combined annotation-dependent depletion) score of 33 (**Fig. 1G**). Thus, the identified variant is predicted to be loss-of-function. Collectively, these data suggest

that this novel homozygous duplication variant of *IL17RC* is causal for the patient's isolated CMC.

Evolutionary and epidemiological genetics of AR IL-17RC deficiency

Among IEI causing isolated CMC, AR IL-17RA deficiency has been reported thus far in 28 cases from 16 kindreds, but AR IL-17RC deficiency has been reported in only four cases, including the current case (Case summary: **Tables S3, S4**) (27,29,30,43–45). We therefore focused on causes of the difference in the frequency of AR IL-17RC deficiency and AR IL-17RA deficiency. We first investigated genomic selection indices to estimate the strength of negative selection at the *IL17RA* and *IL17RC* loci. The consensus score for negative selection (CoNeS), as developed with the combination of several intraspecific and interspecific statistics, was calculated to be 0.73 (top 76.7%) and 1.09 (top 86.9%) for *IL17RA* and *IL17RC*, respectively (**Table S5**) (46). Furthermore, the gene damage index (GDI) values were 11.0 (top 92.0%) and 6.62 (top 78.2%) for *IL17RA* and *IL17RC*, respectively (47). These results indicate that both *IL17RA* and *IL17RC* are not under strong negative selection, with no obvious difference in their selection pressure. Next, we analyzed the frequency of predicted loss-of-function (pLOF) variants in gnomAD. The cumulative frequency of pLOF variants is lower in *IL17RA* than in *IL17RC*, at 1.70×10^{-4} and 1.22×10^{-3}, respectively, even after filtering out a likely benign variant (**Fig. 2B**). Intriguingly, an individual harboring homozygous p.Q378* in *IL17RC*, a variant previously reported to cause isolated CMC, is listed in gnomAD (n=1, allele frequency=4.03×10^{-4}), whereas no homozygous individual for pLOF variants in *IL17RA* was found (**Fig. 2A**).

Abnormal *IL17RC* mRNA and protein expression in patient fibroblasts

We first assessed levels of *IL17RC* mRNA by RT–qPCR in the patient's SV40-immortalized fibroblasts. We found decreased *IL17RC* but not *IL17RA* mRNA expression in her fibroblasts compared to cells from healthy controls or from a patient with AR IL-17RA deficiency (27) (**Fig. 2C, 2D**). These results are comparable to findings for fibroblasts from previously reported patients with homozygous variants (p.Q138*, p.Q378*) of *IL17RC* (30). We next assessed the level of IL-17RC protein expression in the patient's fibroblasts. As in a previous report, immunoblot analysis failed to identify a band specific for IL-17RC in SV40-immortalized fibroblasts from healthy controls and the above-mentioned patients, possibly due to low expression levels of IL-17RC (30). Therefore, as an alternative approach to evaluate the significance of exon13dup *IL17RC* identified in the patient, we transiently transfected the fibroblasts with an empty vector or expression plasmid containing wildtype (WT) or exon13dup *IL17RC* and subsequently assessed protein expression. Cells transfected with the vector plasmid WT IL-17RC showed a band at the expected molecular weight (MW) of 86 kDa corresponding to IL-17RC isoform 1 when using a polyclonal antibody directed against amino acids 113-258 of IL-17RC (**Fig. 2E**). In contrast, a truncated band of approximately 52 kDa was detected in cells transfected with the plasmid encoding exon13dup *IL17RC* (**Fig. 2E**, top panel). Similar findings were obtained using an antibody against the N-terminal V5-

tag (**Fig. 2E**, bottom panel). These results suggest that the duplication variant of *IL17RC* identified in the present patient not only affect mRNA expression, but also influences protein levels if residual expression is present.

Establishment of a functional validation system using *CXCL1* quantitative PCR for *IL17RC* variants

Together with the development of NGS approaches, establishing appropriate evaluation systems for variants of unknown significance has become imperative. However, to date, there is no simple *in vitro* system to validate the pathogenicity of *IL17RC* variants. Currently, patient-derived fibroblasts are used to functionally assess the impact of *IL17RC* variants (30). We thus established an *in vitro* system to functionally assess the impact of *IL17RC* variants by measuring induction of *CXCL1* expression by RT–qPCR in an *IL17RC*-knockout HeLa cell line after 4 hours of stimulation with IL-17A (100 ng/mL). We selected HeLa cells because they are immortalized epithelial tissue cell lines expressing IL-17RA and IL-17RC. The *IL17RC* gene was knocked out using the CRISPR/Cas9 system (for details, see Methods and Materials, **Fig. S1A, S1B**). In this *IL17RC*-knockout HeLa cell system, no *CXCL1* expression was induced after IL-17A stimulation of mock cells, whereas strong induction was observed upon after IL-17A stimulation of cells transfected with WT *IL17RC*. Similarly, cells transfected with any of the gnomAD variants with an MAF > 0.001 or found at a low frequency (MAF ≤ 0.001) but with a CADD score >24 induced high levels of *CXCL1* expression after IL-17A stimulation (**Fig. 1G, 2F**). In marked contrast, no *CXCL1* expression was induced when cells transfected with any of the previously or currently identified *IL17RC* mutant alleles were stimulated with IL-17A (**Fig. 2F**), further demonstrating the deleteriousness of these alleles. These results show the value of such a system in assessing the impact of novel *IL17RC* variants, clearly discriminating between loss-of-function and neutral *IL17RC* variants. Collectively, these findings demonstrate that the novel duplication variant of *IL17RC* identified in the current study is functionally deleterious.

Patient fibroblasts showed abolished responses to IL-17A

We next performed RT–qPCR to assess the response of patient fibroblasts to IL-17A. IL-17A stimulation (100 ng/mL for 2 or 8 hours) induced expression of both *CXCL1* and *IL6* mRNA in fibroblasts from healthy controls but not from the patient carrying the homozygous duplication variant of *IL17RC* (**Fig. 3A, B**). These results are similar to those for fibroblasts from previously reported patients with homozygous *IL17RC* (p.Q138*, p.Q378*) (30) or *IL17RA* (p.Q284*) (27) variants (**Fig. 3A, 3B**). Furthermore, transfecting patient fibroblasts with a plasmid encoding WT but not mutant IL-17RC (isoform 1) restored the response to IL-17A (**Fig. 3C**). Conversely, the response to IL-1β was normal in all of these cells (**Fig. S2A**). Taken together, the lack of response to IL-17A in the patient's SV40-immortalized fibroblasts was rescued by WT IL-17RC expression, confirming this variant to be the

genetic cause of her isolated CMC. We then used 3'-RNA sequencing to further investigate the molecular and functional impact of AR IL-17RC deficiency in response to IL-17A. IL-17A stimulation of healthy control SV40-immortalized fibroblasts upregulated IL-17 signaling pathway-related genes, such as *CXCL1*, *CXCL8*, and *NFKBIZ* (**Fig. 3D**). In contrast, no changes in expression of these genes were observed in the patient's fibroblasts or in fibroblasts from an IL-17RA-deficient patient following stimulation with IL-17A (27) (**Fig. 3D**). IL-1β stimulation upregulated the same pattern of cytokine response-related genes among fibroblasts from healthy subjects and IL-17RC-deficient and IL-17RA-deficient patient (**Fig. 3E**). Enrichment analysis of these upregulated genes showed that the same Gene Ontology terms were enriched in both the control and patient cells, indicating no molecular differences in response to IL-1β (**Fig. S2B**). These data suggest that AR IL-17RC deficiency, similar to AR IL-17RA deficiency, abolishes IL-17A signaling but that these defects do not affect the IL-1β signaling pathway.

Normal differentiation of IL-17-producing T cells and secretion of IL-17 cytokines

We next performed deep immunophenotyping and *in vitro* functional experiments to investigate the detailed immune cell biology of our patient. The numbers and frequencies of her total B cells and B-cell subsets were similar to those in healthy donors (**Fig. S3A-E**). Consistent with intact *in vitro* B-cell maturation *in vivo*, the ability of naïve B cells from the patient to undergo proliferation, Ig class switching, and plasma cell generation in response to T-dependent and T-independent stimuli *in vitro* were also similar to those in healthy controls (**Fig. S3F-H**). Furthermore, frequencies of $CD4^+$ T-cell subsets, such as Th1, Th17, T follicular helper (Tfh), and regulatory T (Treg) cells, were normal, except for a higher frequency of Th17-phenotype cells among all Tfh cells compared to healthy controls (**Fig. S4A-C, S4E-G**). The frequencies of $CD8^+$ T-cell subsets were also similar to those in healthy donors (**Fig. S4B, S4D**). Under *in vitro* differentiation conditions, the proportion of IL-17A-producing memory $CD4^+$ T cells and levels of IL-17A production by these cells were similar between the patient and healthy controls (**Fig. 4C, 4D**). Nevertheless, production of IFN-γ and TNF-a by memory $CD4^+$ T cells was lower in the patient than in healthy donors (**Fig. 4A, S5A**). Finally, although proportions of Th2 phenotype cells in the patient were similar to those in healthy controls, production of Th2 cytokines secreted by memory T cells were higher (**Fig. 4B, S5B**). Overall, distribution of leukocyte subsets and $CD4^+$ T-cell differentiation and function *in vivo* and *ex vivo* in our patient were largely within the dynamic ranges observed for $CD4^+$ T cells from healthy donors, suggesting only a very modest, if any, effect of IL-17RC deficiency on the behavior and function of these cells.

Discussion

We report the fourth patient and the first Asian patient with AR IL-17RC deficiency due to a homozygous novel duplication variant of *IL17RC*. Consistent with previously reported IL-17RC-deficient patients (30), this patient had early-onset mucocutaneous candidiasis but without any other severe infectious diseases, including mucocutaneous *S. aureus* disease or autoimmune clinical signs. This novel variant causes duplication of 46 or 49 bp within exon 13, leading to a frameshift and a premature stop codon at position 457. The patient's fibroblasts exhibited a complete lack of *CXCL1* or *IL6* upregulation after IL-17A stimulation, though this defect was restored by introduction of the WT *IL17RC* allele. We therefore conclude that the homozygous *IL17RC* variant identified in this patient with isolated CMC is a novel pathogenic variant leading to AR IL-17RC deficiency. These results support that IL-17A/F signaling mediated by IL-17RC is essential for mucocutaneous defense against *Candida* but is otherwise redundant for immunity against other pathogens.

Patients with AR IL-17RA or AR ACT1 deficiency frequently develop staphylococcal skin and mucosal infections. Hence, IL-17 immunity is essential for mucocutaneous defense not only against *Candida* but also against *S. aureus* (27–29). On the other hand, mucocutaneous staphylococcal infections were not detected in three previously identified patients (30) or the present patient with AR IL-17RC deficiency. The mechanism for this phenotypic difference remains unclear. Abnormal IL-17E immunity, which is affected in AR IL-17RA deficiency but preserved in AR IL-17RC deficiency, has been suggested but not demonstrated as a plausible mechanism to explain this phenotypic difference (30). Three patients from three generations with CMC, mucocutaneous *S. aureus* infection, and a connective tissue disorder due to AD deficiency of c-Jun N-terminal kinase 1 (JNK1), a component of the MAPK signaling pathway, were recently reported (18). These patients displayed impaired responses to IL-17A and IL-17F and low proportions of Th17 cells but intact responses to IL-17E. A recent study suggested that heterodimers of IL-17RA and IL-17RD function as alternative receptor subunits of IL-17A in primary mouse and human keratinocytes (48). IL-17A signaling is mediated by both IL-17RC and IL-17RD, and the IL-17RA/IL-17RD pathway mainly activates p38 MAPK and JNK (48). These findings suggest that the IL-17RC-independent IL-17RA/IL-17RD pathway may provide the IL-17 immune activity required for protection against infection by *S. aureus* in IL-17RC-deficient patients. Regardless, additional research is needed to fully understand the precise role of IL-17 immunity in mucocutaneous defense against *S. aureus*.

To date, no system has been developed for qualitative evaluation of *IL17RC* variants *in vitro*. In this study, we successfully established a precise *in vitro* assay system using a CRISPR-generated *IL17RC*-knockout HeLa cell line. The system was able to accurately and unambiguously distinguish loss-of-function variants from neutral variants found in public databases and predicted to be functionally intact. In general, increased identification of rare variants through comprehensive approaches in genomic research has emphasized the importance of artificial evaluation systems that accurately assess the impact of variants in the absence of patient-derived samples. In particular, evaluation of *IL17RC* variants requires patient-derived

fibroblasts, making an artificial system even more important. Diagnosis based on accurate evaluation of pathogenicity for identified variants allows for appropriate management and/or treatment of the patient.

AR IL-17RA deficiency is the major genetic cause in patients with isolated CMC due to impaired IL-17 immunity, with 28 cases reported to date. However, only four cases of AR IL-17RC deficiency, including the current case, have been reported thus far. Evolutional and epidemiological genetics analyses revealed no obvious difference in the strength of negative selection at the *IL17RA* and *IL17RC* loci. However, in the general population (gnomAD), the cumulative frequency of pLOF variants is higher for *IL17RC* than *IL17RA*, inconsistent with the fact that the number of patients with AR IL-17RA deficiency identified thus far is higher than that with AR IL-17RC deficiency. These results thus do not explain the observed difference in the incidence of IL-17RA and IL-17RC deficiency. Since many public databases, such as gnomAD, are based on data obtained through whole exome sequence, exon-level duplications observed in our cases, as well as other structural abnormalities like inversions and large deletions, may have been overlooked. This leaves the possibility that the frequency of pathogenic alleles has not been accurately determined. However, the presence of a homozygous p.Q378* variant of *IL17RC* in a public database suggests that undiagnosed mild cases or cases with incomplete penetrance may be expected in individuals with AR IL-17RC deficiency. In contrast, no homozygous deleterious variant of *IL17RA* was found in the public database, suggesting higher penetrance for AR IL-17RA deficiency. If this hypothesis is true, some cases of AR IL-17RC deficiency may not be diagnosed. Further study is needed to fully characterize the cellular, clinical, and frequency differences between AR IL-17RA and IL-17RC deficiencies.

Acknowledgments

We thank the patient and her family for their sincere efforts in cooperating with this study. We also thank Menno van Zelm and Hirokazu Kanegane for help in the breakpoint analysis of the mechanism of the duplication variant, and Masaki Takazawa for technical assistance. The sequence analysis and the single cell sorting were supported by the Analysis Center of Life Science, Natural Science Center for Basic Research and Development, Hiroshima University.

Statements and Declarations

Funding

SO is supported by the Japan Society for the Promotion of Science (JSPS) KAKENHI (grant Numbers: 19H03620, 22H03041, 18KK0228 and 22KK0113) and the Japan Agency for Medical Research and Development (AMED) (grant Number: JP23ek0109623, JP22ek0109480). MT is supported by MEXT/JSPS KAKENHI (grant Numbers: 22K15921) JLC is supported by National Institutes of Health (grant Numbers: R01AI127564). SGT and CSM are supported by Investigator Grants awarded by the National Health and Medical Research Council of Australia, and project grants from the Allergy & Immunology Foundation of Australia, and the Job Research Foundation. AP is supported by the Integrative Biology of Emerging Infectious Diseases Laboratoire d′Excellence (ANR-10-LABX-62-IBEID), the French National Research Agency (ANR) (grant no. GENCMCD-ANR-11-BSV3-005-01, no. HGDIFD-ANR-14-CE15-0006-01, no. EURO-CMC-ANR-14-RARE-0005-02), the National Institute of Allergy and Infectious Diseases of the National Institutes of Health (grant no. U01AI109697 and no. R01AI127564).

Disclosure of potential conflict of interest

The authors declare that they have no relevant conflicts of interest.

Data availability

The datasets generated during and/or analysed during the current study are available from the corresponding author on reasonable request.

Authorship Contribution

SO designed and supervised the study. KN wrote the manuscript with support from TA, JLC, AP, SGT and SO. TS, KI, MT, YI, YM, SK, SH, and YL contributed to sample preparation and provision of clinical information. KN, MT, and TN carried out the experiments. CSM designed and supervised

experiments and analyzing data. FS, JH, and OO analyzed the data. All authors contributed to manuscript preparation, read, and approved the final manuscript.

Ethics Statement

This study was approved by the Ethics Committee/Internal Review Board of Hiroshima University. All experiments were carried out with adherence to the Declaration of Helsinki.

Consent to participate

Written informed consent was obtained from the patient’s parent.

Consent for publication

Consent to submission of the case report to the journal was obtained from the patient's parent.

References

1. Kirkpatrick CH, Hill HR. Chronic mucocutaneous candidiasis. Pediatr Infect Dis J. 2001 Feb;20(2):197–206. DOI:https://doi.org/10.1097/00006454-200102000-00017
2. Puel A, Cypowyj S, Maródi L, Abel L, Picard C, Casanova JL. Inborn errors of human IL-17 immunity underlie chronic mucocutaneous candidiasis. Curr Opin Allergy Clin Immunol. 2012 Dec;12(6):616–22. DOI:https://doi.org/10.1097/ACI.0b013e328358cc0b
3. Puel A, Picard C, Cypowyj S, Lilic D, Abel L, Casanova JL. Inborn errors of mucocutaneous immunity to Candida albicans in humans: a role for IL-17 cytokines? Curr Opin Immunol. 2010 Aug;22(4):467–74. DOI:https://doi.org/10.1016/j.coi.2010.06.009
4. Puel A. Human inborn errors of immunity underlying superficial or invasive candidiasis. Hum Genet. 2020 Jun;139(6–7):1011–22. DOI:https://doi.org/10.1007/s00439-020-02141-7
5. Okada S, Puel A, Casanova JL, Kobayashi M. Chronic mucocutaneous candidiasis disease associated with inborn errors of IL-17 immunity. Clin Transl Immunol. 2016 Dec;5(12):e114. DOI:https://doi.org/10.1038/cti.2016.71
6. De Beaucoudtey L, Puel A, Filipe-Santos O, Cobat A, Ghandil P, Chrabieh M, et al. Mutations in STAT3 and IL12RB1 impair the development of human IL-17-producing T cells. J Exp Med. 2008;205(7):1543–50. DOI:https://doi.org/10.1084/jem.20080321
7. Ma CS, Chew GYJ, Simpson N, Priyadarshi A, Wong M, Grimbacher B, et al. Deficiency of Th17 cells in hyper IgE syndrome due to mutations in STAT3. J Exp Med. 2008;205(7):1551–7. DOI:https://doi.org/10.1084/jem.20080218
8. Milner JD, Brenchley JM, Laurence A, Freeman AF, Hill BJ, Elias KM, et al. Impaired TH17 cell differentiation in subjects with autosomal dominant hyper-IgE syndrome. Nature. 2008;452(7188):773–6. DOI:https://doi.org/10.1038/nature06764
9. Chandesris MO, Melki I, Natividad A, Puel A, Fieschi C, Yun L, et al. Autosomal dominant STAT3 deficiency and hyper-IgE syndrome: Molecular, cellular, and clinical features from a french national survey. Med (United States). 2012;91(4):1–19. DOI:https://doi.org/10.1097/MD.0b013e31825f95b9
10. Béziat V, Tavernier SJ, Chen YH, Ma CS, Materna M, Laurence A, et al. Dominant-negative mutations in human IL6ST underlie hyper-IgE syndrome. J Exp Med. 2020;217(6). DOI:https://doi.org/10.1084/jem.20191804
11. Béziat V, Li J, Lin JX, Ma CS, Li P, Bousfiha A, et al. A recessive form of hyper-IgE syndrome by disruption of ZNF341-dependent STAT3 transcription and activity. Sci Immunol. 2018;3(24). DOI:https://doi.org/10.1126/SCIIMMUNOL.AAT4956
12. Frey-Jakobs S, Hartberger JM, Fliegauf M, Bossen C, Wehmeyer ML, Neubauer JC, et al. ZNF341 controls STAT3 expression and thereby immunocompetence. Sci Immunol. 2018 Jun

15;3(24):1–7. DOI:https://doi.org/10.1126/sciimmunol.aat4941

13. Okada S, Asano T, Moriya K, Boisson-Dupuis S, Kobayashi M, Casanova JL, et al. Human STAT1 Gain-of-Function Heterozygous Mutations: Chronic Mucocutaneous Candidiasis and Type I Interferonopathy. J Clin Immunol. 2020;40(8):1065–81. DOI:https://doi.org/10.1007/s10875-020-00847-x
14. Liu L, Okada S, Kong XF, Kreins AY, Cypowyj S, Abhyankar A, et al. Gain-of-function human STAT1 mutations impair IL-17 immunity and underlie chronic mucocutaneous candidiasis. J Exp Med. 2011;208(18):1635–48. DOI:https://doi.org/10.1084/jem.20110958
15. Depner M, Fuchs S, Raabe J, Frede N, Glocker C, Doffinger R, et al. The Extended Clinical Phenotype of 26 Patients with Chronic Mucocutaneous Candidiasis due to Gain-of-Function Mutations in STAT1. J Clin Immunol. 2016;36(1):73–84. DOI:https://doi.org/10.1007/s10875-015-0214-9
16. Toubiana J, Okada S, Hiller J, Oleastro M, Gomez ML, Becerra JCA, et al. Heterozygous STAT1 gain-of-function mutations underlie an unexpectedly broad clinical phenotype. Blood. 2016;127(25):3154–64. DOI:https://doi.org/10.1182/blood-2015-11-679902
17. Mizoguchi Y, Okada S. Inborn errors of STAT1 immunity. Curr Opin Immunol. 2021;72:59–64. DOI:https://doi.org/10.1016/j.coi.2021.02.009
18. Li J, Ritelli M, Ma CS, Rao G, Habib T, Corvilain E, et al. Chronic mucocutaneous candidiasis and connective tissue disorder in humans with impaired JNK1-dependent responses to IL-17A/F and TGF-β. Sci Immunol. 2019;4(41):139–48. DOI:https://doi.org/10.1126/sciimmunol.aax7965
19. De Beaucoudrey L, Samarina A, Bustamante J, Cobat A, Boisson-Dupuis S, Feinberg J, et al. Revisiting human IL-12Rβ1 deficiency: A survey of 141 patients from 30 countries. Medicine (Baltimore). 2010;89(6):381–402. DOI:https://doi.org/10.1097/MD.0b013e3181fdd832
20. Philippot Q, Ogishi M, Bohlen J, Puchan J, Arias AA, Nguyen T, et al. Human IL-23 is essential for IFN-γ-dependent immunity to mycobacteria. Sci Immunol [Internet]. 2023 Feb 17 [cited 2023 Feb 16];8(80):eabq5204. DOI:https://doi.org/10.1126/sciimmunol.abq5204
21. Ouederni M, Sanal O, Ikincioğullari A, Tezcan I, Dogu F, Sologuren I, et al. Clinical features of candidiasis in patients with inherited interleukin 12 receptor β1 deficiency. Clin Infect Dis. 2014;58(2):204–13. DOI:https://doi.org/10.1093/cid/cit722
22. Glocker EO, Hennigs A, Nabavi M, Schäffer AA, Woellner C, Salzer U, et al. A Homozygous CARD9 Mutation in a Family with Susceptibility to Fungal Infections. N Engl J Med. 2009;361(18):1727–35. DOI:https://doi.org/10.1056/nejmoa0810719
23. Lanternier F, Pathan S, Vincent QB, Liu L, Cypowyj S, Prando C, et al. Deep dermatophytosis and inherited CARD9 deficiency. N Engl J Med. 2013 Oct 31;369(18):1704–14. DOI:https://doi.org/10.1056/NEJMoa1208487
24. Corvilain E, Casanova JL, Puel A. Inherited CARD9 Deficiency: Invasive Disease Caused by

Ascomycete Fungi in Previously Healthy Children and Adults. J Clin Immunol. 2018 Aug;38(6):656–93. DOI:https://doi.org/10.1007/s10875-018-0539-2

25. Okada S, Markle JG, Deenick EK, Mele F, Averbuch D, Lagos M, et al. IMMUNODEFICIENCIES. Impairment of immunity to Candida and Mycobacterium in humans with bi-allelic RORC mutations. Science. 2015 Aug 7;349(6248):606–13. DOI:https://doi.org/10.1126/science.aaa4282
26. Li J, Vinh DC, Casanova JL, Puel A. Inborn errors of immunity underlying fungal diseases in otherwise healthy individuals. Curr Opin Microbiol. 2017 Dec 1;40:46–57. DOI:https://doi.org/10.1016/J.MIB.2017.10.016
27. Puel A, Cypowyj S, Bustamante J, Wright JF, Liu L, Lim HK, et al. Chronic mucocutaneous candidiasis in humans with inborn errors of interleukin-17 immunity. Science. 2011 Apr 1;332(6025):65–8. DOI:https://doi.org/10.1126/science.1200439
28. Boisson B, Wang C, Pedergnana V, Wu L, Cypowyj S, Rybojad M, et al. An ACT1 mutation selectively abolishes interleukin-17 responses in humans with chronic mucocutaneous candidiasis. Immunity. 2013;39(4):676–86. DOI:https://doi.org/10.1016/j.immuni.2013.09.002
29. Lévy R, Okada S, Béziat V, Moriya K, Liu C, Chai LYA, et al. Genetic, immunological, and clinical features of patients with bacterial and fungal infections due to inherited IL-17RA deficiency. Proc Natl Acad Sci U S A. 2016;113(51):E8277–85. DOI:https://doi.org/10.1073/pnas.1618300114
30. Ling Y, Cypowyj S, Aytekin C, Galicchio M, Camcioglu Y, Nepesov S, et al. Inherited IL-17RC deficiency in patients with chronic mucocutaneous candidiasis. J Exp Med. 2015;212(5):619–31. DOI:https://doi.org/10.1084/jem.20141065
31. Marujo F, Pelham SJ, Freixo J, Cordeiro AI, Martins C, Casanova JL, et al. A Novel TRAF3IP2 Mutation Causing Chronic Mucocutaneous Candidiasis. J Clin Immunol. 2021;41(6):1376–9. DOI:https://doi.org/10.1007/s10875-021-01026-2
32. Shafer S, Yao Y, Comrie W, Cook S, Zhang Y, Yesil G, et al. Two patients with chronic mucocutaneous candidiasis caused by TRAF3IP2 deficiency. J Allergy Clin Immunol. 2021 Jul;148(1):256-261.e2. DOI:https://doi.org/10.1016/j.jaci.2020.12.629
33. Bhattad S, Dinakar C, Pinnamaraju H, Ganapathy A, Mannan A. Chronic Mucocutaneous Candidiasis in an Adolescent Boy Due to a Novel Mutation in TRAF3IP2. J Clin Immunol. 2019;39(6):596–9. DOI:https://doi.org/10.1007/s10875-019-00664-x
34. Li J, Casanova JL, Puel A. Mucocutaneous IL-17 immunity in mice and humans: Host defense vs. excessive inflammation. Mucosal Immunol. 2018;11(3):581–9. DOI:https://doi.org/10.1038/mi.2017.97
35. Gaffen SL. Structure and signalling in the IL-17 receptor family. Nat Rev Immunol. 2009;9(8):556–67. DOI:https://doi.org/10.1038/nri2586

36. Li X, Bechara R, Zhao J, McGeachy MJ, Gaffen SL. IL-17 receptor–based signaling and implications for disease. Vol. 20, Nature Immunology. 2019. p. 1594–602. DOI:https://doi.org/10.1038/s41590-019-0514-y
37. Monaco G, Lee B, Xu W, Mustafah S, Hwang YY, Carré C, et al. RNA-Seq Signatures Normalized by mRNA Abundance Allow Absolute Deconvolution of Human Immune Cell Types. Cell Rep. 2019;26(6):1627-1640.e7. DOI:https://doi.org/10.1016/j.celrep.2019.01.041
38. Iwakura Y, Ishigame H, Saijo S, Nakae S. Functional Specialization of Interleukin-17 Family Members. Immunity. 2011;34(2):149–62. DOI:https://doi.org/10.1016/j.immuni.2011.02.012
39. Fujiki R, Ikeda M, Yoshida A, Akiko M, Yao Y, Nishimura M, et al. Assessing the Accuracy of Variant Detection in Cost-Effective Gene Panel Testing by Next-Generation Sequencing. J Mol Diagn. 2018 Sep 1;20(5):572–82. DOI:https://doi.org/10.1016/j.jmoldx.2018.04.004
40. Naito Y, Hino K, Bono H, Ui-Tei K. CRISPRdirect: software for designing CRISPR/Cas guide RNA with reduced off-target sites. Bioinformatics. 2015 Apr 1;31(7):1120–3. DOI:https://doi.org/10.1093/BIOINFORMATICS/BTU743
41. Ran FA, Hsu PD, Wright J, Agarwala V, Scott DA, Zhang F. Genome engineering using the CRISPR-Cas9 system. Nat Protoc. 2013 Nov;8(11):2281–308. DOI:https://doi.org/10.1038/nprot.2013.143
42. Ho AW, Shen F, Conti HR, Patel N, Childs EE, Peterson AC, et al. IL-17RC is required for immune signaling via an extended SEF/IL-17R signaling domain in the cytoplasmic tail. J Immunol. 2010 Jul 15;185(2):1063–70. DOI:https://doi.org/10.4049/jimmunol.0903739
43. Aujnarain A, Dadi H, Mandola A. Chronic mucocutaneous candidiasis associated with a novel frameshift mutation in IL-17 receptor alpha. LymphoSign J. 2019;6(2):68–74. DOI:https://doi.org/10.14785/lymphosign-2019-0007
44. Frede N, Rojas-Restrepo J, Caballero Garcia de Oteyza A, Buchta M, Hübscher K, Gámez-Díaz L, et al. Genetic Analysis of a Cohort of 275 Patients with Hyper-IgE Syndromes and/or Chronic Mucocutaneous Candidiasis. J Clin Immunol. 2021 Nov;41(8):1804–38. DOI:https://doi.org/10.1007/s10875-021-01086-4
45. Kılıç M, Özcan MH, Taşkın E, Şen A. A family with interleukin-17 receptor A deficiency: a case report and review of the literature. Turk J Pediatr. 2023;65(1):135–43. DOI:https://doi.org/10.24953/turkjped.2022.40
46. Rapaport F, Boisson B, Gregor A, Béziat V, Boisson-Dupuis S, Bustamante J, et al. Negative selection on human genes underlying inborn errors depends on disease outcome and both the mode and mechanism of inheritance. Proc Natl Acad Sci U S A. 2021;118(3):1–9. DOI:https://doi.org/10.1073/pnas.2001248118
47. Itan Y, Shang L, Boisson B, Patin E, Bolze A, Moncada-Vélez M, et al. The human gene damage index as a gene-level approach to prioritizing exome variants. Proc Natl Acad Sci U S A.

2015;112(44):13615–20. DOI:https://doi.org/10.1073/pnas.1518646112

48. Su Y, Huang J, Zhao X, Lu H, Wang W, Yang XO, et al. Interleukin-17 receptor D constitutes an alternative receptor for interleukin-17A important in psoriasis-like skin inflammation. Sci Immunol. 2019;4(36):1–16. DOI:https://doi.org/10.1126/sciimmunol.aau9657

Figure legends

Figure 1. CMCD patient with AR IL-17RC deficiency. A, Pedigree of the family established by *IL17RC* genotyping. A sporadic case of CMCD without a family history of CMCD. The proband is indicated by an arrow. The black symbol represents an individual with CMCD. "E?" indicates individuals for whom genetic analysis was not possible. **B**, Pictures of the oral and esophageal candidiasis of the patient. The left picture represents oral candidiasis at the age of seven years, and the right picture represents esophageal candidiasis at the same age. **C**, Panel testing of next-generation sequencing (NGS). Schematic representation indicating an increased number of reads in a region including the entire exon 13 of *IL17RC* by IGV software. **D**, Sanger sequencing chromatograms of the *IL17RC* region harboring a duplication variant (Chr3: 9,971,476-9,971,606 dup (+131bp)) for the proband and family members. **E,** Protein-level representations of the patient's variant for both duplications of 46 and 49 bases (p.D458Afs*16 and p.D458Afs*17). **F,** Schematic representation of the IL-17RC protein, with its signal sequence (SS), extracellular (EC), transmembrane (TM), intracellular (IC), and SEFIR (similar expression to fibroblast growth factor genes and IL-17R) domains and the positions affected by variants (our variant is shown in red). **G,** Predicted CADD scores (GRCh37-v1.6, https://cadd.gs.washington.edu/) and global allele frequencies of *IL17RC* variants, for which homozygotes are reported in the gnomAD database (v2.1.1). A red dot shows our patient's variant (CADD score 33); blue dots show previously reported *IL17RC*-LOF variants.

Figure 2. Epidemiological genetics of *IL17RC* and *IL17RA*. A and B, MAF and CADD scores (GRCh37-v1.6) for pLOF variants of the (A) *IL17RC* and (B) *IL17RA* genes in the gnomAD database (v2.1.1). The red dot shows previously reported *IL17RC*-LOF variants. **Impaired production of *IL17RC* mRNA and protein with the *IL17RC* duplication mutant allele. C and D,** mRNA levels of *IL17RC* (C) and *IL17RA* (D) in SV40-immortalized fibroblasts from controls, the patient, IL-17RC-deficient individuals (R138* and R378*) and an IL-17RA-deficient individual, as detected by the TaqMan assay. *GAPDH* was used for normalization as an endogenous control. Error bars represent SEM (n = 3). The results shown are representative of three independent experiments. Statistical analysis was performed using one-way ANOVA with Tukey's post hoc test. *: $p < 0.001$. **E,** Immunoblotting of total protein extracts from patient fibroblasts transfected with the empty pUNO1mcs vector (mock) or the pUNO1 plasmid encoding the WT or exon13dup IL-17RC protein. IL-17RC was detected with an anti-IL-17RC antibody (recognizes amino acids 113-258) or an antibody against the N-terminal V5-tag. Gray triangles represent the targeted bands. These experiments were repeated at least three times. **New *in vitro* system for functional validation of *IL17RC* variants. F,** Induction of *CXCL1* expression in *IL17RC*-knockout HeLa cells transfected with an empty vector (mock) or an IL-17RC plasmid encoding WT or each of the mutants (exon13dup_1, 2, Q138*, R376*, Q378*, or polymorphisms reported in public databases) after

4 hours of stimulation with 100 ng/mL IL-17A, as determined by the TaqMan assay. *GAPDH* was used for normalization as an endogenous control. The results shown are representative of three independent experiments. Error bars represent SEM (n = 3).

Figure 3. Patient-derived SV-40-immortalized fibroblasts fail to respond to IL-17A stimulation. A and B, Induction of *CXCL1* (A) and *IL6* (B) expression in SV40-immortalized fibroblasts from controls, the patient, IL-17RC-deficient individuals (R138* and Q378*) and an IL-17RA-deficient individual after 2 or 8 hours of stimulation with 100 ng/mL IL-17A, as determined by the TaqMan assay. The results are representative of three independent experiments. Error bars represent SEM (n = 3). **C,** Complementation of fibroblasts from patients with the WT *IL17RC* allele. *CXCL1* induction by SV40-immortalized fibroblasts from the patient transfected with an empty vector (mock) or an IL-17RC plasmid encoding WT or exon13dup mutants after 2 or 8 h of stimulation with 100 ng/mL IL-17A, as determined by the TaqMan assay. *GAPDH* was used for normalization as an endogenous control. The data shown represent mean values from three independent experiments. Error bars represent SEM (n = 3). Statistical analysis was performed using one-way ANOVA with Dunnett's multiple comparison test. *: $p < 0.05$. **D and E,** MA plot analysis of RNA sequencing data of SV40-immortalized fibroblast from controls, the patient, and an IL-17RA-deficient individual. MA plot showing log2-transformed average signal versus log2-fold change by IL-17A (D) or IL-1β (E) stimulation in each cell. Red dots show genes with upregulated expression (>1.0) in fibroblasts from controls (n = 2). The X-axis shows average expression (unstimulated and IL-17A or IL-1β stimulated), and the Y-axis represents the difference in expression between unstimulated and IL-17A- or IL-1β-stimulated cells.

Figure 4. *In vitro* functional characterization of $CD4^+$ Th cells with AR IL-17RC deficiency. A-D, Secretion of IL-2, Th1 (IFN-γ and TNF) (A), Th2 (IL-4, IL-5, and IL-13) (B), and Th17 (IL- 17A, IL-17F, and IL-22) (C) cytokines by memory $CD4^+$ T cells and frequency of Th17 (IL-17A, IL-17F, and IL-22) cytokine-positive memory $CD4^+$ T cells (D) after 5 days of stimulation with T-cell activation and expansion beads (anti-CD2/CD3/CD28) alone (Th0) or under Th1 (IL-12)-, Th2 (IL-4)-, or Th17 (TGF-β, IL-1β, IL-6, IL-21, and IL-23)-polarizing conditions. Error bars represent SEM. Black dots show healthy controls, blue squares show the heterozygous carrier mother, and red triangles show the patient with AR IL-17RC deficiency.

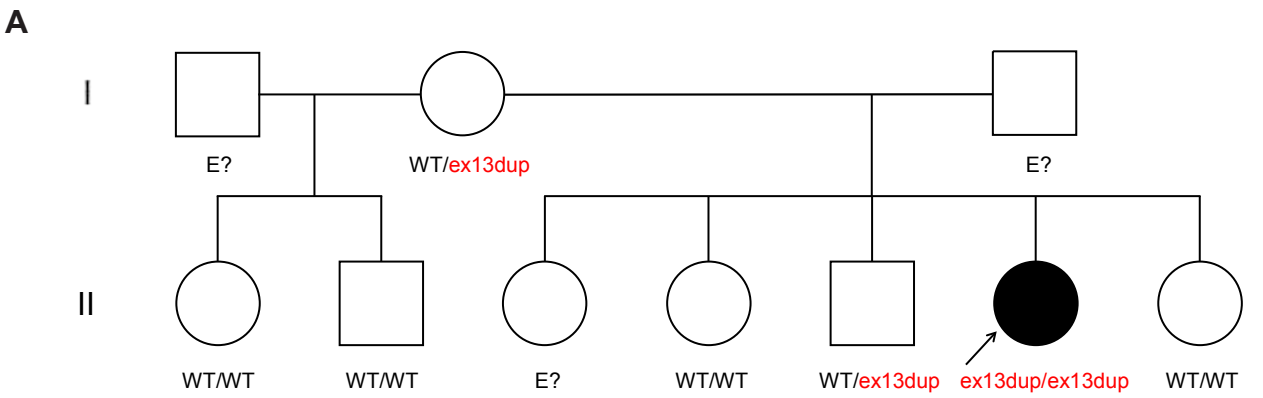
A
I
II
E?
WT/ex13dup
E?
WT/WT
WT/WT
E?
WT/WT
WT/ex13dup
ex13dup/ex13dup
WT/WT


B

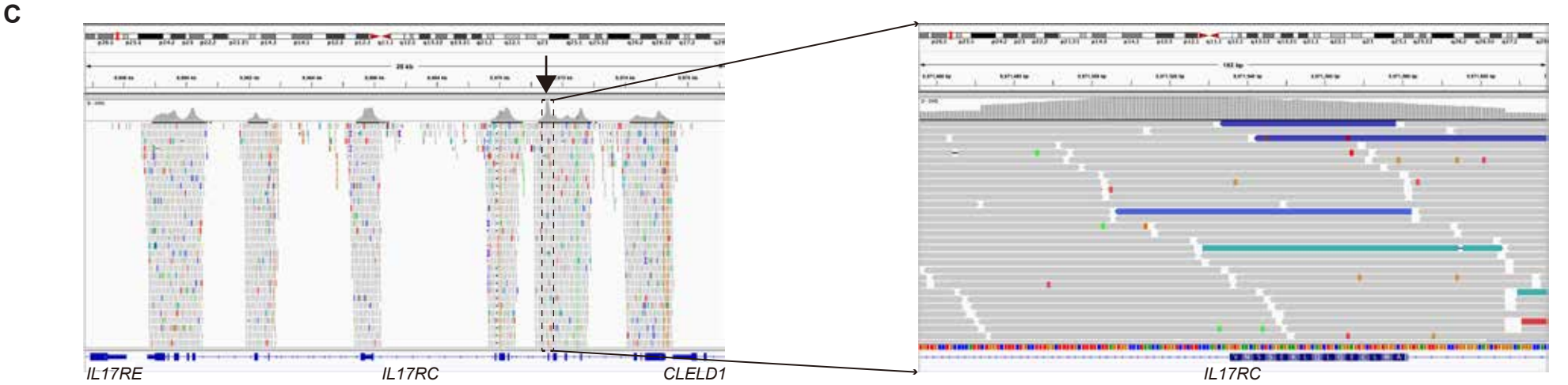
C
IL17RE
IL17RC
CLELD1
IL17RC

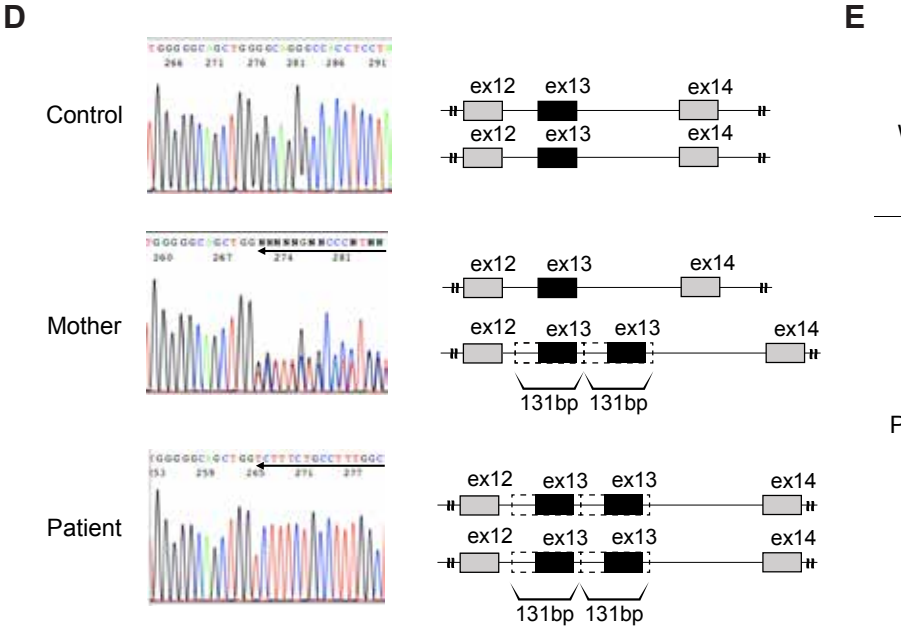
D
Control
Mother
Patient
ex12
ex13
ex14
ex13
131bp
131bp

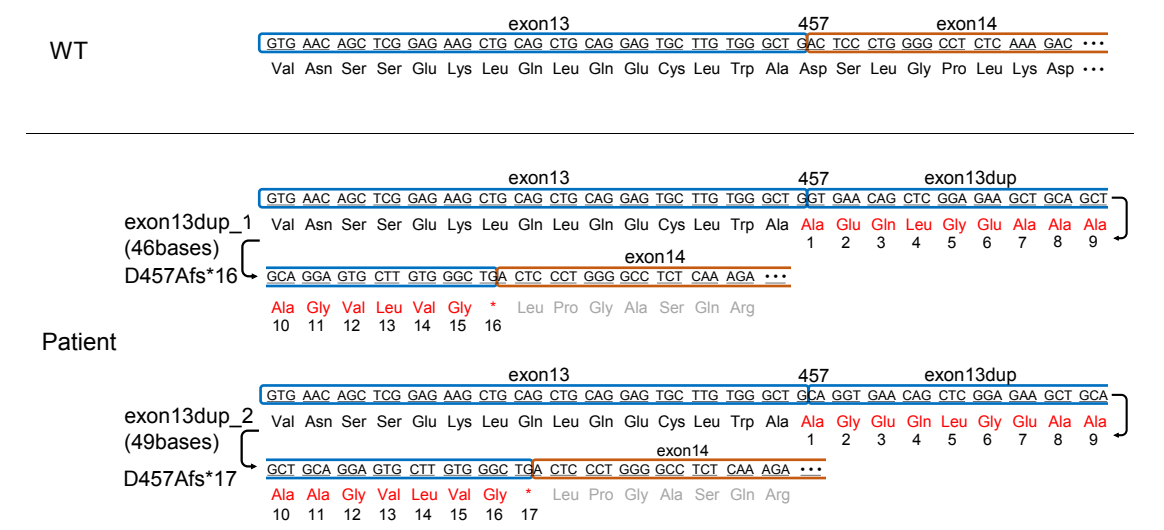
E
WT
exon13
457
exon14
GTG AAC AGC TCG GAG AAG CTG CAG CTG CAG GAG TGC TTG TGG GCT GAC TCC CTG GGG CCT CTC AAA GAC
Val Asn Ser Ser Glu Lys Leu Gln Leu Gln Glu Cys Leu Trp Ala Asp Ser Leu Gly Pro Leu Lys Asp
Patient
exon13dup_1
(46bases)
D457Afs*16
exon13
457
exon13dup
exon14
Ala Gly Val Leu Val Gly * Leu Pro Gly Ala Ser Gln Arg
exon13dup_2
(49bases)
D457Afs*17
Ala Ala Gly Val Leu Val Gly * Leu Pro Gly Ala Ser Gln Arg

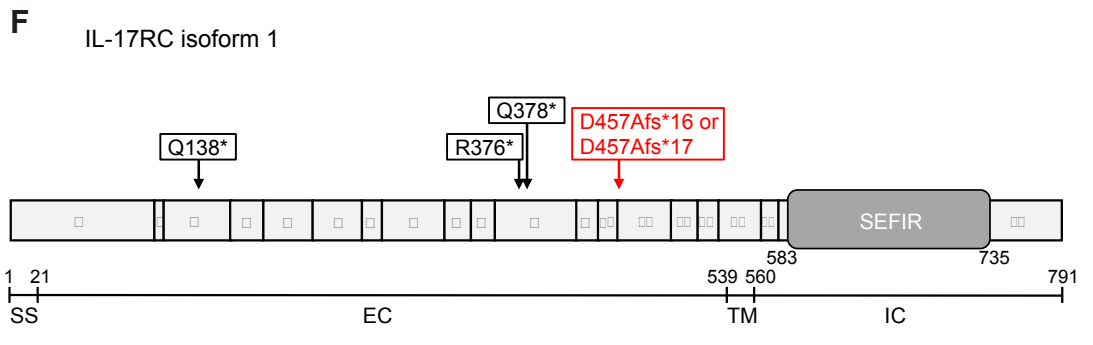
F
IL-17RC isoform 1
Q138*
R376*
Q378*
D457Afs*16 or
D457Afs*17
SEFIR
1
21
539
560
583
735
791
SS
EC
TM
IC

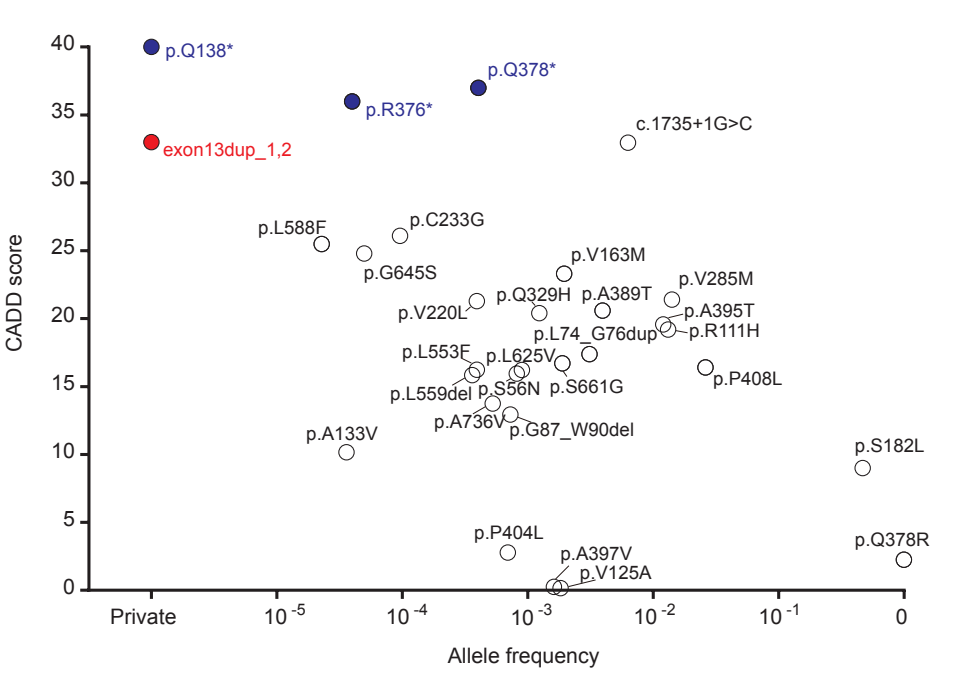
G
CADD score
Allele frequency
Private
p.Q138*
p.Q378*
p.R376*
exon13dup_1,2
c.1735+1G>C
p.L588F
p.C233G
p.G645S
p.V163M
p.V285M
p.Q329H
p.A389T
p.V220L
p.A395T
p.L74_G76dup
p.R111H
p.L553F
p.L625V
p.P408L
p.L559del
p.S56N
p.S661G
p.A736V
p.G87_W90del
p.A133V
p.S182L
p.P404L
p.A397V
p.V125A
p.Q378R

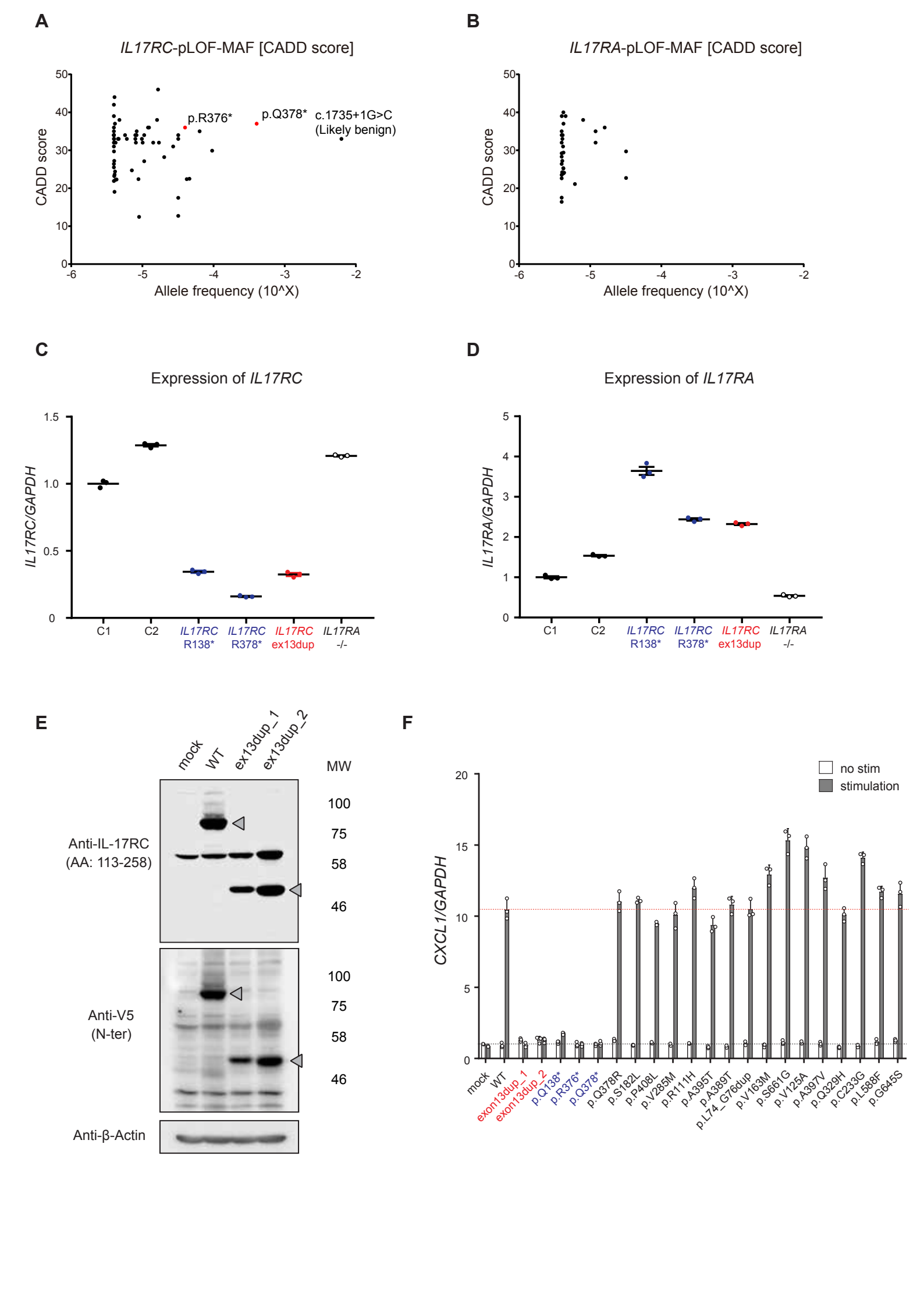
A
IL17RC-pLOF-MAF [CADD score]
CADD score
Allele frequency (10^X)
p.R376*
p.Q378*
c.1735+1G>C
(Likely benign)
B
IL17RA-pLOF-MAF [CADD score]
CADD score
Allele frequency (10^X)
C
Expression of IL17RC
IL17RC/GAPDH
C1
C2
IL17RC R138*
IL17RC R378*
IL17RC ex13dup
IL17RA -/-
D
Expression of IL17RA
IL17RA/GAPDH
C1
C2
IL17RC R138*
IL17RC R378*
IL17RC ex13dup
IL17RA -/-
E
mock
WT
ex13dup_1
ex13dup_2
MW
Anti-IL-17RC (AA: 113-258)
Anti-V5 (N-ter)
Anti-β-Actin
F
no stim
stimulation
CXCL1/GAPDH
mock
WT
exon13dup_1
exon13dup_2
p.Q138*
p.R376*
p.Q378*
p.Q378R
p.S182L
p.P408L
p.V285M
p.R111H
p.A395T
p.A389T
p.L74_G76dup
p.V163M
p.S661G
p.V125A
p.A397V
p.Q329H
p.C233G
p.L588F
p.G645S

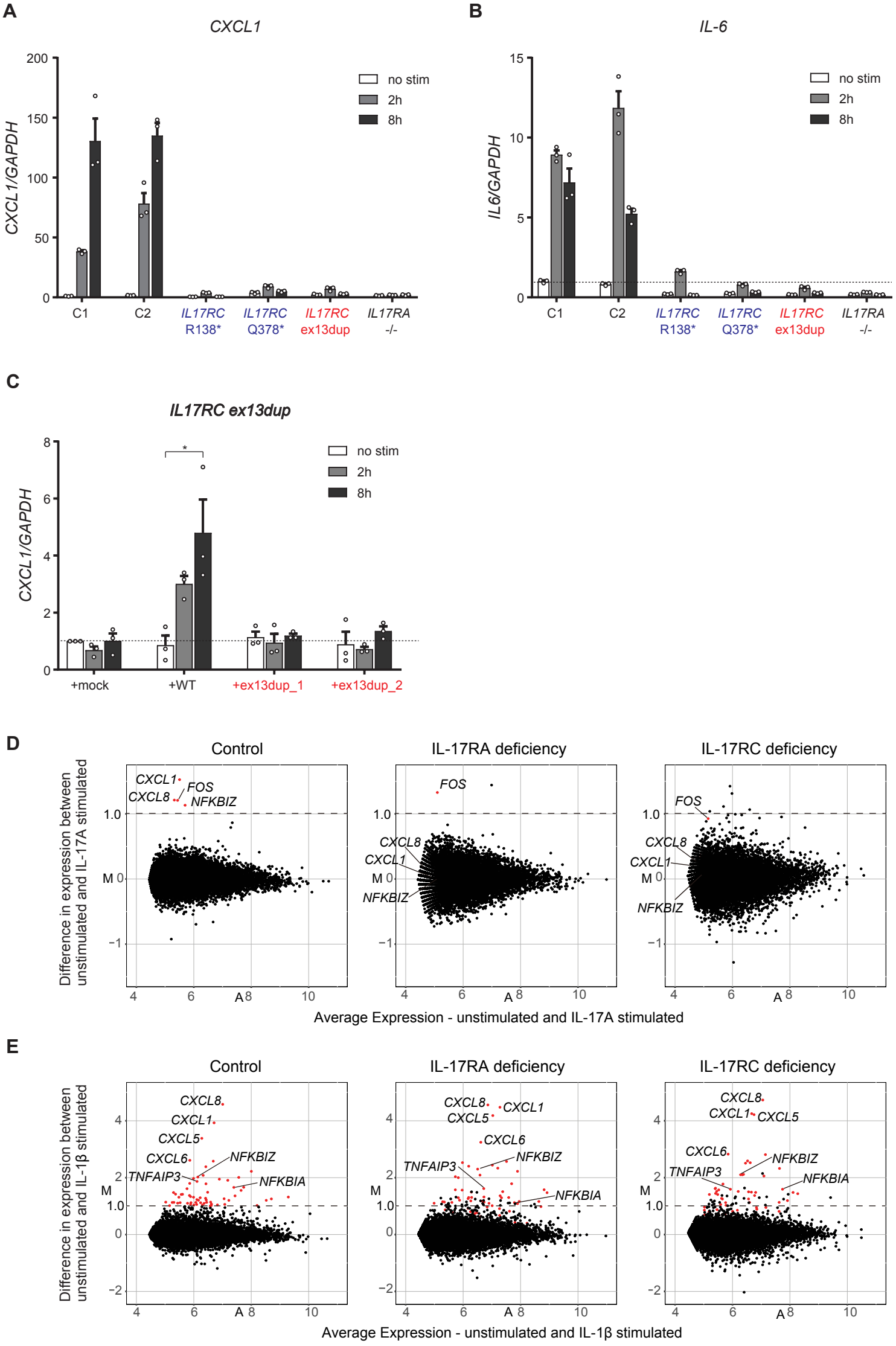
A
CXCL1
CXCL1/GAPDH
200
150
100
50
0
no stim
2h
8h
C1
C2
IL17RC R138*
IL17RC Q378*
IL17RC ex13dup
IL17RA -/-
B
IL-6
IL6/GAPDH
15
10
5
0
C
IL17RC ex13dup
*
+mock
+WT
+ex13dup_1
+ex13dup_2
D
Control
IL-17RA deficiency
IL-17RC deficiency
Difference in expression between unstimulated and IL-17A stimulated
CXCL1
CXCL8
FOS
NFKBIZ
M
A
Average Expression - unstimulated and IL-17A stimulated
E
Control
IL-17RA deficiency
IL-17RC deficiency
Difference in expression between unstimulated and IL-1β stimulated
CXCL8
CXCL1
CXCL5
CXCL6
TNFAIP3
NFKBIZ
NFKBIA
Average Expression - unstimulated and IL-1β stimulated

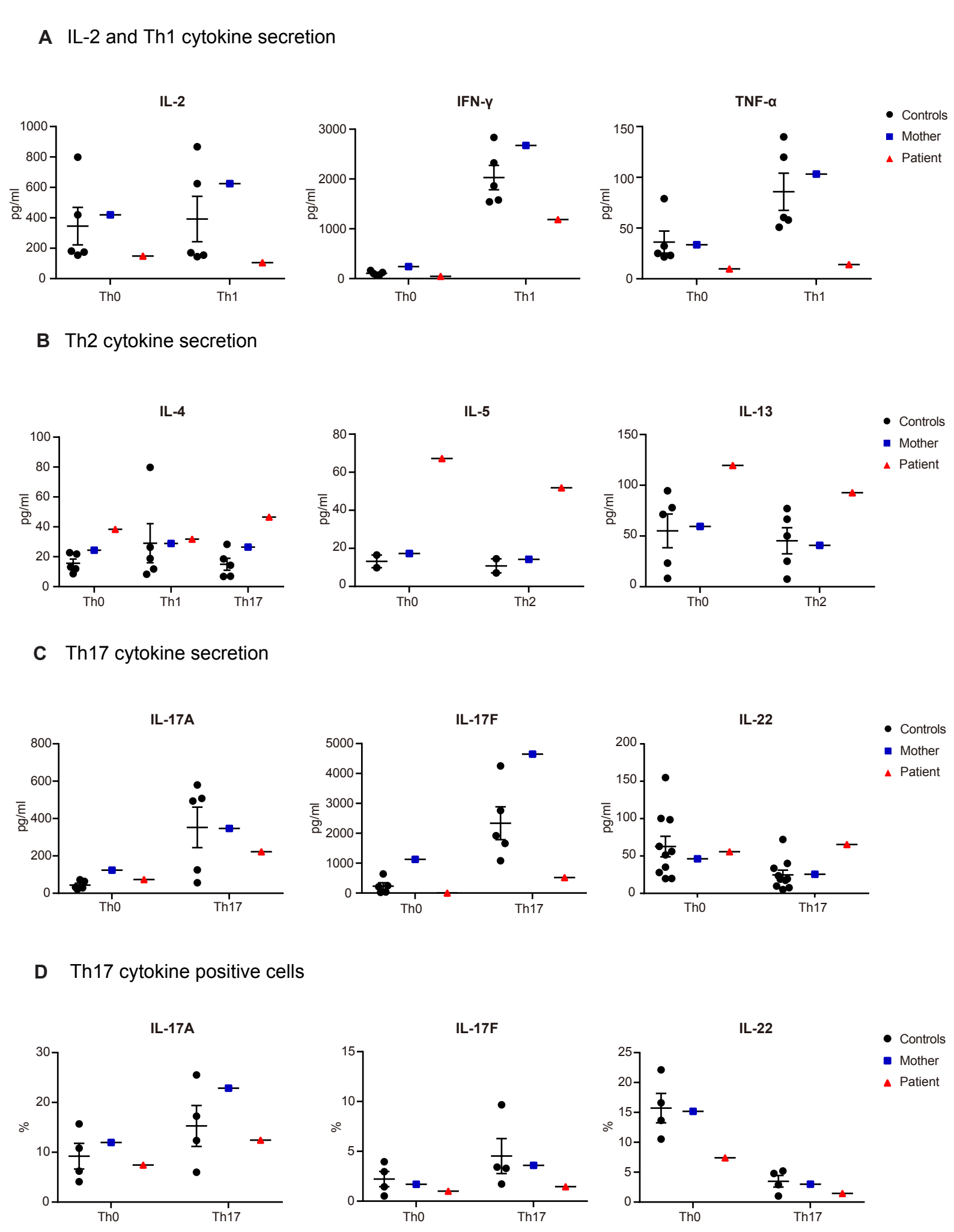
A IL-2 and Th1 cytokine secretion
IL-2
IFN-γ
TNF-α
pg/ml
Th0
Th1
Controls
Mother
Patient
B Th2 cytokine secretion
IL-4
IL-5
IL-13
Th0
Th1
Th17
Th2
C Th17 cytokine secretion
IL-17A
IL-17F
IL-22
D Th17 cytokine positive cells
%

Supplementary Materials

Methods

Mutagenesis and Transient Transfections

We used the pUNO1-V5 expression vectors containing WT or *IL17RC* mutants. The vector encoding *IL17RC* exon13dup was generated as follows. RNA extracted from patient SV40-fibroblasts was synthesized into cDNA, which was amplified by PCR using primers targeting the full length of *IL17RC*. The PCR product was introduced into pTA2 vector by TA-cloning and then reintroduced into V5-taggerd pUNO1vector using restriction enzymes. The expression vectors encoding other *IL17RC* mutants were generated with PCR-based mutagenesis of the pUNO1-V5 WT *IL17RC* vector with mismatched PCR primers. The primer sequences and PCR conditions are available upon request. These vectors were transfected into fibroblasts or HeLa cells with Lipofectamine® LTX Reagent (Thermo Fisher Scientific, Waltham, MA, USA).

Cell culture

Immortalized SV40-fibroblasts and HeLa cell were grown in complete DMEM supplemented with 10% heat-inactivated FBS. Cells were incubated at 37°C in the presence of 5% CO2.

Fibroblast activation

SV40-fibroblasts were plated in 6-well plates at a density of $2x10^5$ cells/well. The cells were incubated for 24 hours and were then transfected with mock, the pUNO1 vector coding, WT or *IL17RC* mutants (2.5 μg). After 24 hours, the transfected cells were left unstimulated or were stimulated with recombinant human 100 ng/ml IL-17A or 10 ng/ml IL-1β (R&D Systems) for 2 or 8 hours.

3′ mRNA-seq library preparation and analysis

TRIzol reagent (Thermo Fisher) was used for RNA extraction, and an Agilent 2100 Bioanalyzer (Agilent Technologies, Santa Clara, CA, USA) was used to confirm RNA concentration and quality. A total of 500 ng of RNA was used for 3′ mRNA library preparation according to the manufacturer's protocol using the QuantSeq 3′ mRNA-Seq Library Prep Kit FWD (LEXOGEN). After a 12-cycle PCR process, the RNA library was sequenced using an Illumina NextSeq 500 system (75 cycles; San Diego, CA, USA). FASTQ files were created from the reads using bcl2fastq ver2.17 (Illumina). The quality

of the FASTQ sequence data was evaluated using FastQC v0.11.9 (Illumina). Adaptor sequences were removed from the raw RNA-seq reads. The trimmed reads were aligned to the GRCh38 human reference genome using STAR v2.7.6a. The identified genes that did not contain missing values were included in the analysis and their expression levels were normalized by variance stabilizing normalization method using the R package NormalyzerDE (1). R software (https://cran.r-project.org/) was used to depict MA plots, and Metascape was used for function enrichment analysis (2).

Deep immunophenotyping

Freshly thawed PBMCs were washed, passed through a 35µM strainer, then stained using Zombie Aqua™ viability dye (Biolegend) according to the manufacturer's protocols. Cells were labelled in the presence of Brilliant Stain Buffer (BD Biosciences) with the following anti-human mAbs: anti-CD3 BV570, anti-CCR7 PECy7, anti-CXCR3 BV421, anti-TCR Vα7.2 APC-Cy7 (all from Biolegend); anti-CD20 BUV805, anti-CD4 BUV661, anti-CD8 BUV496, anti-CD10 BV650, anti-CD27 BB515, anti-CD45RA BUV395, anti-CXCR5 BUV615-P, IgG BB660-P2, anti-TCR-Vγδ BV711, anti-CD161 BV786 (all from BD Biosciences); anti-CD21 BUV563, IgA1/IgA2 PE-Cy5, anti-CCR6 BB630-P (all custom from BD Biosciences). Following thorough washing, samples were fixed with 1% formalin and acquired on the FACSymphony™ A5 (BD Biosciences). Data was analysed using FlowJo software (Tree Star). Frequencies of B and T lymphocytes, as well as subpopulations, were determined using gating strategies published previously (3).

Assessment of cell division history

CFSE-labelled naive B cells ($CD20^+CD10^-CD27^-$) were cultured at a density of 150-200x10^3 cells/ml in 96-well round bottom plates with 200ng/ml CD40L crosslinked to 50ng/ml HA (R&D systems) alone or together with 100U/ml IL-4 (DNAX) and/ or 50ng/ml IL-21 (PeproTech). Plates were incubated at 37°C with 5% CO_2. After 5 days, cells were harvested and stained with Zombie Aqua viability dye (BioLegend) and analyzed on the BD LSRFortessa (BD Biosciences). CFSE dilution was analyzed on Zombie-negative cells.

Assessment of plasmablast formation and class switching

Sorted naïve B cells ($CD20^+CD10^-CD27^-$) were cultured at a density of 150x10^3 cells/mL in 96-well round bottom tissue culture plates with 200ng/ml CD40L crosslinked to 50ng/ml HA (R&D systems) alone or together with 100U/ml IL-4 (DNAX) and/or 50ng/ml IL-21 (PeproTech). Plates were incubated at 37°C with 5% CO_2. After 5 days,

cells were stained with Zombie Aqua viability dye (BioLegend) to distinguish live cells, then labelled with anti-human mAbs – anti-CD27 PECy7, anti-CD38 APC, anti-IgG BV605 (all from BD Biosciences) – to distinguish plasmablasts and class-switched cells.

Statistical analysis

Values of $p < 0.05$ were considered significant. Data were tested for statistical significance with R (version 4.2.1).

References

1. Willforss J, Chawade A, Levander F. NormalyzerDE: Online Tool for Improved Normalization of Omics Expression Data and High-Sensitivity Differential Expression Analysis. J Proteome Res. 2019 Feb 1;18(2):732–40. DOI:https://doi.org/10.1021/acs.jproteome.8b00523
2. Zhou Y, Zhou B, Pache L, Chang M, Khodabakhshi AH, Tanaseichuk O, et al. Metascape provides a biologist-oriented resource for the analysis of systems-level datasets. Nat Commun. 2019 Apr 3;10(1):1523. DOI:https://doi.org/10.1038/s41467-019-09234-6
3. Payne K, Li W, Salomon R, Ma CS. OMIP-063: 28-Color Flow Cytometry Panel for Broad Human Immunophenotyping. Cytom Part A. 2020;97(8):777–81. DOI:https://doi.org/10.1002/cyto.a.24018

Supplemental Figure legends

Figure S1. Confirmation of *IL17RC*-knockout HeLa cells. A, Sanger sequencing of *IL17RC*-knockout HeLa cell clones showing a compound heterozygous frameshift deletion (40bp or 73bp). **B,** mRNA levels for *IL17RC* in *IL17RC*-knockout HeLa cells, as detected by the TaqMan assay. GAPDH was used for normalization as an endogenous control. Errors bars represent SEM (n = 3). The results are representative of three independent experiments. **PCR targeted exon13 of *IL17RC* on cDNA from patient's peripheral blood. C,** A band was observed at the predicted position (436 bp) in the control, but at a longer length in the patient.

Figure S2. Normal response of patient fibroblasts to IL-1β. A, *CXCL1* induction by SV40-fibroblast from the patient transfected with an empty vector (mock) or an IL-17RC vector encoding the WT or exon13dup mutants, after 2 or 8 h of stimulation with 100 ng/ml IL-1β, as determined by TaqMan assay. GAPDH was used for normalization as an endogenous control. Data shown represents mean values from three independent experiments. Errors bars represent SEM (n = 3). **B**, **Enrichment analysis of RNA-seq data.** Genes upregulated by stimulation with IL-17A or IL-1β in fibroblasts from controls, IL17RA-deficient or IL17RC-deficient cells were analyzed by Metascape.

Figure S3. Normal B-cell subsets in the patient. A-E, Frequencies of B cells (CD20+) **(A)**, transitional (CD20+CD10+CD27-), naïve (CD20+CD10-CD27-), memory (CD20+CD10-CD27+) B cells **(B)**, IgG^+ or IgA^+ cells among switched memory B cells **(C)**, unswitched memory B cells **(D)**, and CD21 low B cells **(E)**. White bars show healthy controls, blue bars show heterozygous carrier mother, and red bars show the patient with AR IL-17RC deficiency. **Normal proliferation, plasmablast formation, and class switching of naïve B cells in the patient. F-H,** CFSE-labeled naive B cells were cultured with CD40L alone or in the presence of IL-21 or IL-21 and IL-4. After 5 days, the percentage of cells in each division **(F)** was determined from the CFSE profiles and the percentage of plasmablasts ($CD27^{hi}CD38^{hi}$) **(G)** and IgG-expressing cells **(H)** were determined by flow cytometry. Black dots show healthy controls, blue dots show the heterozygous carrier mother, and red dots show the patient with AR IL-17RC deficiency.

Figure S4. T cell immunophenotyping in the patient. Frequencies of $CD3^+$ cells **(A)**,

$CD4^+$ T cells (CD3+CD4+) or $CD8^+$ T cells (CD3+CD8+) **(B)**. Frequency of naive (CD45RA+CCR7+), central memory (CD45RA-CCR7+), effector memory (CD45RA-CCR7-), or EMRA (CD45RA+CCR7-) cells among the $CD4^+$ T cells **(C)** and $CD8^+$ T cells **(D)**. Frequency of naïve cells (CXCR5-CD45RA+), non-Tfh memory cells (CXCR5-CD45RA-), Tfh cells (CXCR5+, CD45RA-), or Treg cells ($CD25^{hi}CD127^{lo}$) among $CD4^+$ T cells **(E)**. Frequency of Th1 (CXCR3+CCR6-) or TH17 (CXCR3-CCR6+) subsets among non-Tfh memory cells **(F)** and Tfh cells **(G)**. White bars show healthy controls, blue bars show the heterozygous carrier mother, and red bars show the patient with AR IL-17RC deficiency.

Figure S5. T-cell differentiation in the patient. Frequency of IL-2, Th1 (IFN-γ and TNF) **(A)** and Th2 (IL-4 and IL-13) **(B)** cytokine-positive memory $CD4^+$ T cells after 5 d of stimulation with T cell activation and expansion beads (anti-CD2/CD3/CD28) alone (Th0) or under Th1 (IL-12) or Th2 (IL-4) polarizing conditions. Black dots show healthy controls, blue squares show the heterozygous carrier mother, and red triangles show the patient with AR IL-17RC deficiency.

A

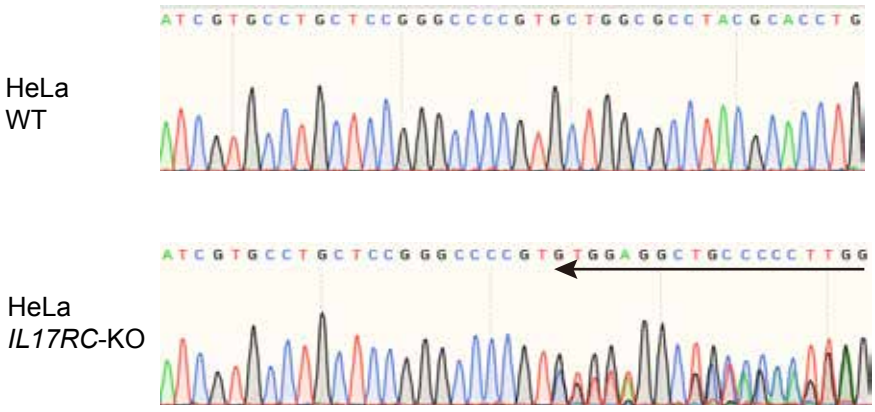
HeLa
WT
HeLa
IL17RC-KO

B

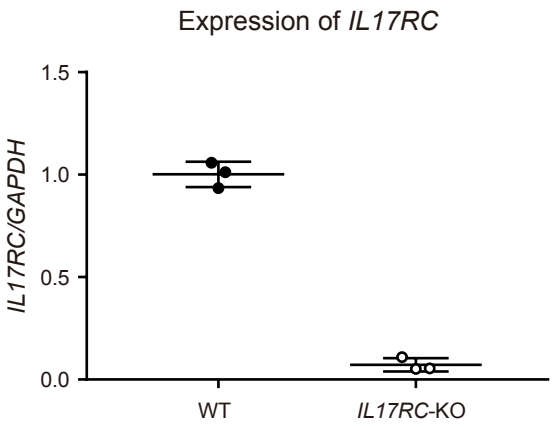
Expression of IL17RC
IL17RC/GAPDH
1.5
1.0
0.5
0.0
WT
IL17RC-KO

C

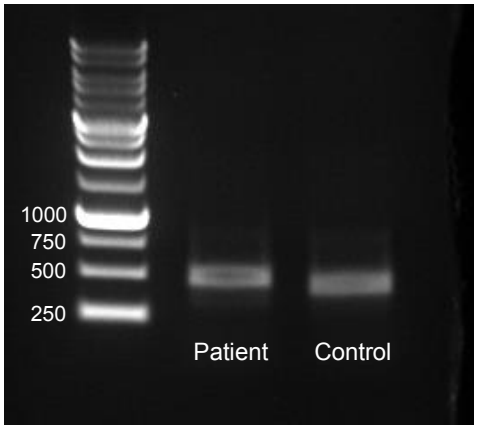
1000
750
500
250
Patient
Control

A

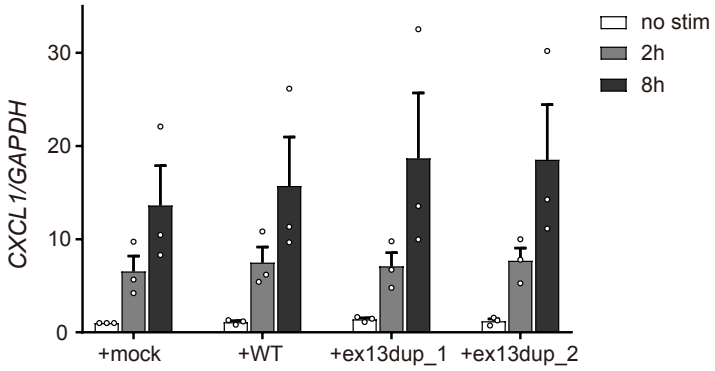

B

IL-17A Stimulation

IL-1β Stimulation

Control

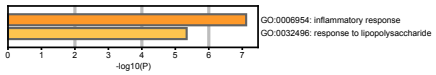

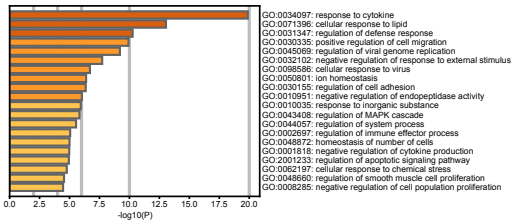

IL-17RA deficiency

There is no enriched GO term.

(Min Overlap:3, P Value Cutoff:0.01)

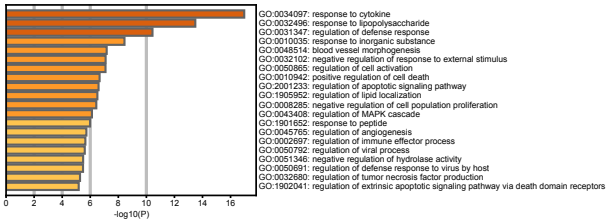

IL-17RC deficiency

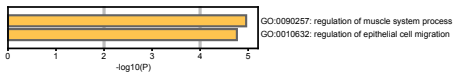

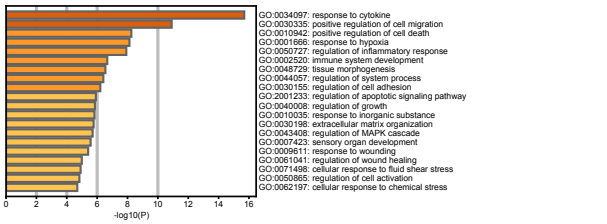

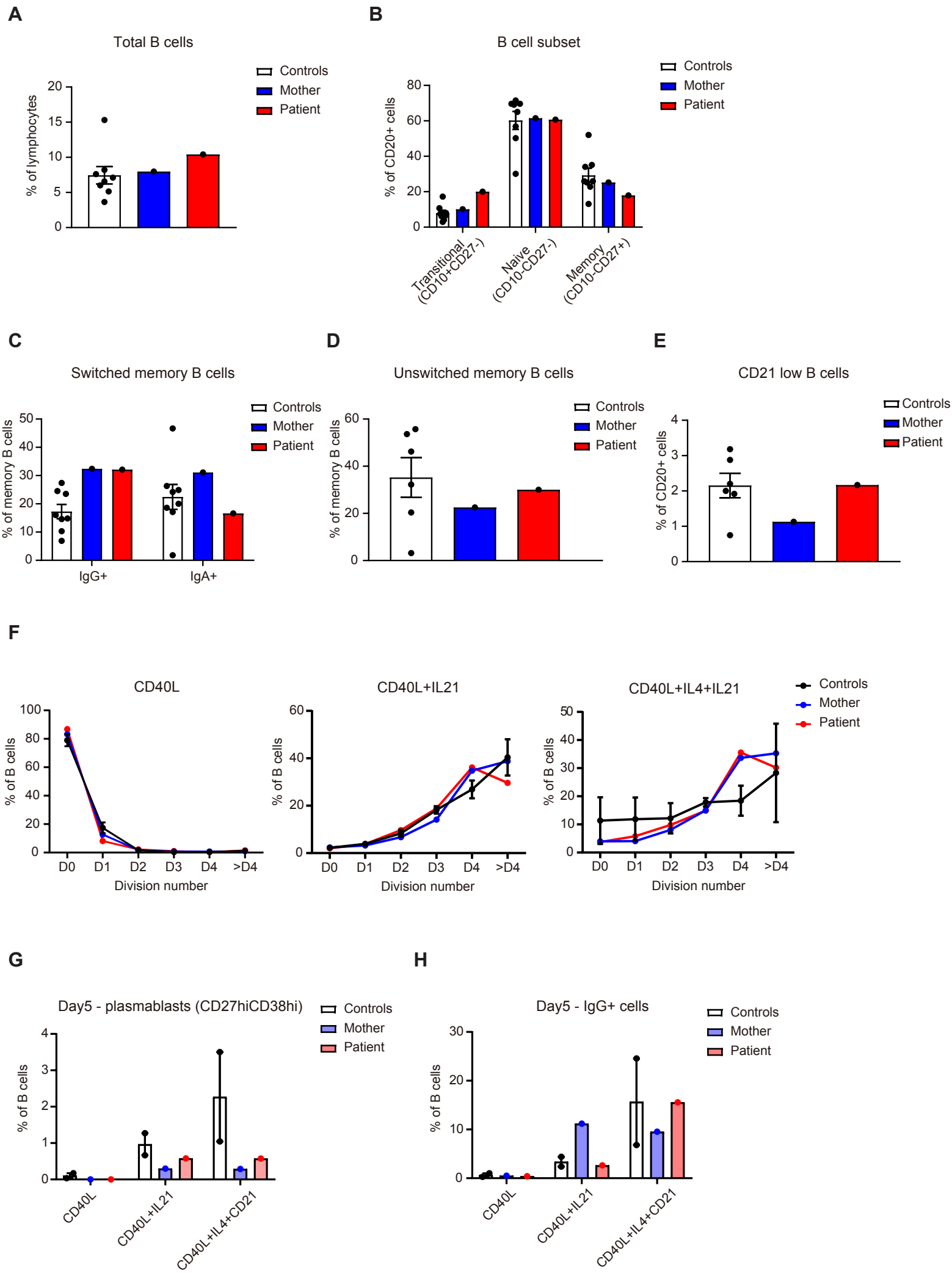
A
Total B cells
% of lymphocytes
20
15
10
5
0
Controls
Mother
Patient
B
B cell subset
% of CD20+ cells
80
60
40
20
0
Transitional (CD10+CD27-)
Naive (CD10-CD27-)
Memory (CD10-CD27+)
Controls
Mother
Patient
C
Switched memory B cells
% of memory B cells
50
40
30
20
10
0
IgG+
IgA+
Controls
Mother
Patient
D
Unswitched memory B cells
% of memory B cells
60
40
20
0
Controls
Mother
Patient
E
CD21 low B cells
% of CD20+ cells
4
3
2
1
0
Controls
Mother
Patient
F
CD40L
CD40L+IL21
CD40L+IL4+IL21
% of B cells
100
80
60
40
20
0
D0
D1
D2
D3
D4
>D4
Division number
Controls
Mother
Patient
G
Day5 - plasmablasts (CD27hiCD38hi)
% of B cells
4
3
2
1
0
CD40L
CD40L+IL21
CD40L+IL4+CD21
Controls
Mother
Patient
H
Day5 - IgG+ cells
% of B cells
30
20
10
0
CD40L
CD40L+IL21
CD40L+IL4+CD21
Controls
Mother
Patient

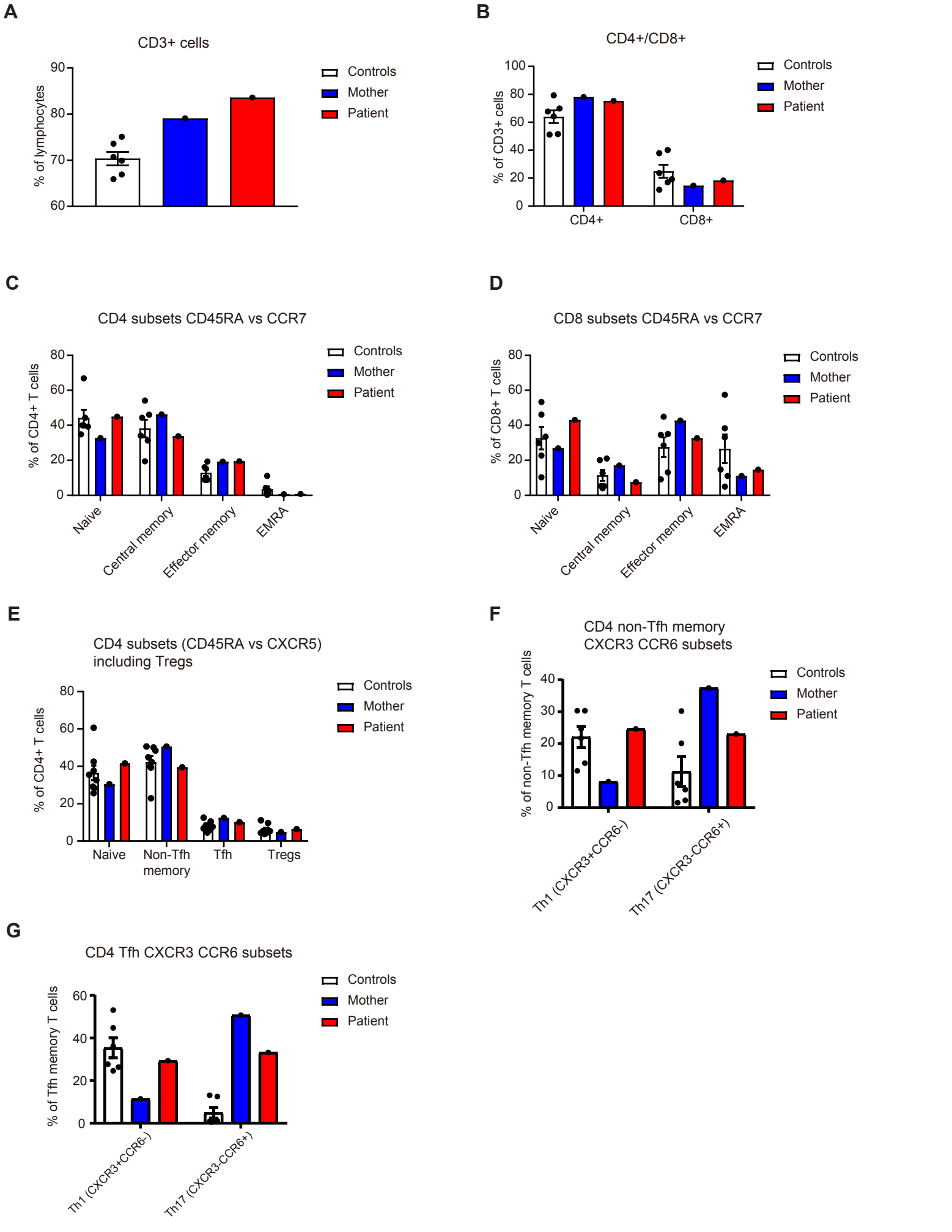
A
CD3+ cells
% of lymphocytes
90
80
70
60
Controls
Mother
Patient
B
CD4+/CD8+
% of CD3+ cells
100
80
60
40
20
0
CD4+
CD8+
Controls
Mother
Patient
C
CD4 subsets CD45RA vs CCR7
% of CD4+ T cells
80
60
40
20
0
Naive
Central memory
Effector memory
EMRA
Controls
Mother
Patient
D
CD8 subsets CD45RA vs CCR7
% of CD8+ T cells
80
60
40
20
0
Naive
Central memory
Effector memory
EMRA
Controls
Mother
Patient
E
CD4 subsets (CD45RA vs CXCR5)
including Tregs
% of CD4+ T cells
80
60
40
20
0
Naive
Non-Tfh memory
Tfh
Tregs
Controls
Mother
Patient
F
CD4 non-Tfh memory
CXCR3 CCR6 subsets
% of non-Tfh memory T cells
40
30
20
10
0
Th1 (CXCR3+CCR6-)
Th17 (CXCR3-CCR6+)
Controls
Mother
Patient
G
CD4 Tfh CXCR3 CCR6 subsets
% of Tfh memory T cells
60
40
20
0
Th1 (CXCR3+CCR6-)
Th17 (CXCR3-CCR6+)
Controls
Mother
Patient

A IL-2 and Th1 cytokine positive cells

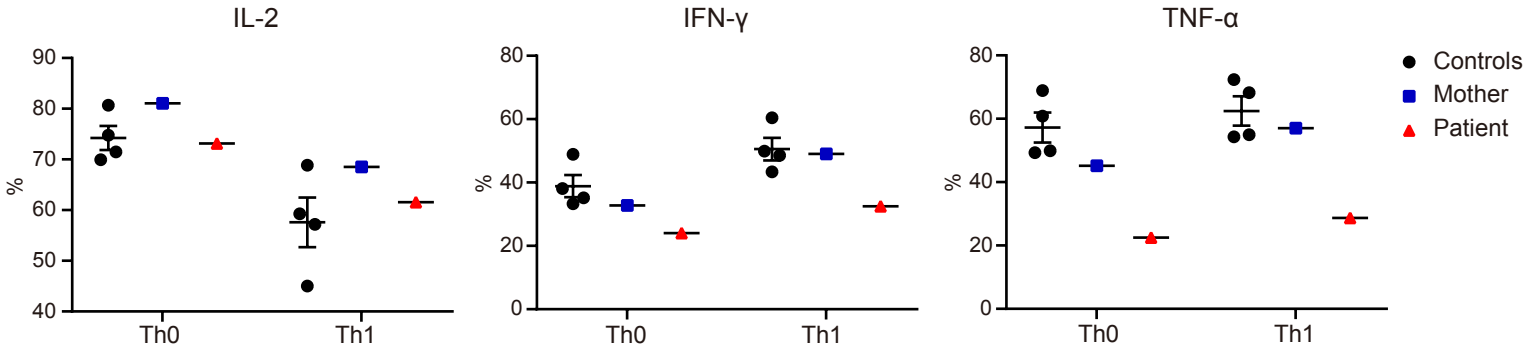

B Th2 cytokine positive cells